NATIONAL ENERGY TECHNOLOGY LABORATORY

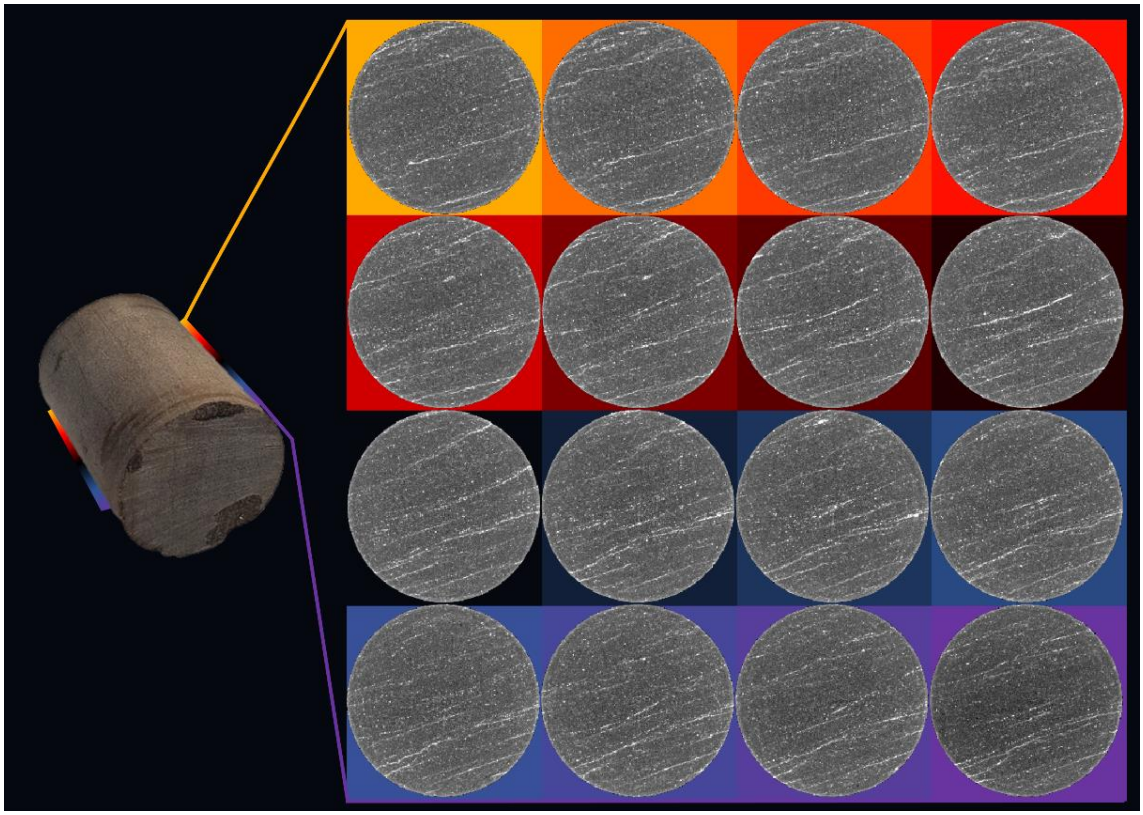

Computed Tomography Scanning and Geophysical Measurements of the Fayetteville Shale Formation from the Nixon B #1-7 Well

29 March 2022

U.S. DEPARTMENT OF ENERGY | NATIONAL ENERGY TECHNOLOGY LABORATORY

Office of Fossil Energy and Carbon Management

DOE/NETL-2022/3728

Disclaimer

This project was funded by the United States Department of Energy, National Energy Technology Laboratory, in part, through a site support contract.

Cover Illustration: Core photo (left) and micro-CT image montage (right) of Nixon B #1-7, 1 in. sub-core at 3,130.4 ft with gradient color to denote the location of reslice within the sub-core.

Suggested Citation: Paronish, T.; Schmitt, R.; Moore, J.; Jarvis, K.; Brown, S.; Dotson, B.; Crandall, D. *Computed Tomography Scanning and Geophysical Measurements of the Fayetteville Shale Formation from the Nixon B #1-7 Well;* DOE.NETL-2022.3728; NETL Technical Report Series; U.S. Department of Energy, National Energy Technology Laboratory: Morgantown, WV, 2022; p 44. DOI: 10.2172/1859751

An electronic version of this report can be found at:

https://netl.doe.gov/energy-analysis/search

https://edx.netl.doe.gov/ucr

The data in this report can be accessed from NETL's Energy Data eXchange (EDX) online system (https://edx.netl.doe.gov) using the following link:
https://edx.netl.doe.gov/dataset/nixonb-1-7

Computed Tomography Scanning and Geophysical Measurements of the Fayetteville Shale Formation from the Nixon B #1-7 Well

Thomas Paronish[1,2], Rhiannon Schmitt[1,3], Johnathan Moore[1,2], Karl Jarvis[1,2], Sarah Brown[1,2], Ben Dotson[4], Dustin Crandall[1]

[1]U.S. Department of Energy, National Energy Technology Laboratory, 3610 Collins Ferry Road, Morgantown WV 26507

[2]NETL Support Contractor, 3610 Collins Ferry Road, Morgantown WV 26507

[3]U.S. Department of Energy, Oak Ridge Institute for Science and Education, 3610 Collins Ferry Road, Morgantown WV 26507

[4]Southwestern Energy, 10000 Energy Drive, Spring TX 77389

DOE/NETL-2022/3728

29 March 2022

NETL Contacts:

Dustin Crandall, Principal Investigator

Eilis Rosenbaum and Christina Lopano, Technical Portfolio Leads

Bryan Morreale, Executive Director, Research & Innovation Center

This page intentionally left blank.

Table of Contents

This page intentionally left blank.

List of Figures

List of Figures (cont.)

List of Tables

Acronyms, Abbreviations, and Symbols

Term	Description
2D	Two-dimensional
3D	Three-dimensional
CT	Computed tomography
CTN	CT number
DOE	U.S. Department of Energy
EDX	NETL's Energy Data eXchange
HU	Hounsfield Units
MSCL	Multi-Sensor Core Logger
NETL	National Energy Technology Laboratory
XRF	X-ray fluorescence

Acknowledgments

This work was completed at the National Energy Technology Laboratory (NETL) with support from U.S. Department of Energy's (DOE) Office of Fossil Energy and Carbon Management Oil & Gas Program. The authors wish to acknowledge Bryan Morreale, Alexandra Hakala, Christina Lopano, and Eilis Rosenbaum (NETL Research & Innovation Center), Jared Ciferno, (NETL Technology Development and Integration Center), and Elena Melchert (DOE Office of Fossil Energy and Carbon Management) for programmatic guidance, direction, and support.

The authors would like to thank Bryan Tennant and Scott Workman for data collection and technical support. This research was supported in part by appointments from the NETL Research Participation Program, sponsored by the U.S. DOE and administered by the Oak Ridge Institute for Science and Education (ORISE).

ABSTRACT

The computed tomography (CT) facilities and the Multi-Sensor Core Logger (MSCL) at the National Energy Technology Laboratory (NETL) in Morgantown, West Virginia were used to characterize core from the Fayetteville and Pitkin formations. This core came from a vertical well drilled by Southwestern Energy (Nixon B #1-7 well) and characterized as part of the U.S. Department of Energy's (DOE) Fossil Energy and Carbon Management Onshore portfolio's focus on unconventional shale plays.

The primary impetus of this work is to characterize Fayetteville Shale core, from an unconventional shale play in Northwestern Arkansas, that is relatively under-reported on when compared to larger unconventional resources in the continental U.S. This report, and the associated scans, provide detailed datasets not typically made publicly available from unconventional shales for analysis. The resultant datasets are presented in this report and can be accessed from NETL's Energy Data eXchange online system using the following link: https://edx.netl.doe.gov/dataset/nixonb-1-7.

All equipment and techniques used were non-destructive, enabling future examinations and analyses to be performed on these cores. None of the equipment used was suitable for direct visualization of the shale pore space, although fractures and discontinuities were detectable with the methods tested. Coarse resolution CT imagery with the NETL medical CT scanner was performed on the entire core and two zones of potential interest. Qualitative analysis of the medical CT images, coupled with X-ray fluorescence, P-wave, and magnetic susceptibility measurements from the MSCL were useful in identifying zones of interest for more detailed analysis as well as fractured zones. The ability to quickly identify key areas for more detailed study with higher resolution will save time and resources in future studies. The combination of methods used provided a multi-scale analysis of this core and provided both a macro and micro description of the core that is relevant for many subsurface energy-related examinations that have traditionally been performed at NETL.

1. INTRODUCTION

Evaluation of core data from ongoing and emerging unconventional reservoirs has long been a priority of the U.S. Department of Energy's (DOE) National Energy Technology Laboratory (NETL). In fulfillment of this mission, the goal of this report is to characterize and disseminate data from the Nixon B #1-7 well, a well in the western portion of the Fayetteville Play. This report builds on the techniques of previous core characterization technical reports and aims to meet the growing demand for high quality and comprehensive lithological data.

The primary objective for this study was to characterize core from an unconventional reservoir in a growing and emerging field, utilizing methods not available to most researchers. The computed tomography (CT) and the Multi-Sensor CoreLogger (MSCL) at NETL in Morgantown, West Virginia, provides a means to characterize the well and disseminate the data to the public in several formats in this report and through NETL's Energy Data eXchange (EDX)(https://edx.netl.doe.gov/dataset/nixonb-1-7). Little detailed analysis is presented in this report, but simply presents the data available for others to utilize and develop, and creates an enhanced digital representation of the core data.

1.1 STUDY AREA

The Nixon B #1-7 well (API 03-047-11288-00-00) was drilled in the summer of 2004 in the B-43 field in Franklin County, Arkansas (Latitude: 35.551; Longitude: -94.009) and targeted the Fayetteville Formation. Core was retrieved from the top of the Pitkin Limestone to the base of the Fayetteville Shale, and it is made up of 170.5 ft of core in two nearly contiguous sections (3,060–3,134 ft; 3,200–3,306.5 ft).

1.2 GEOLOGICAL SETTING

The late Mississippian (Chesterian) (345 Ma) Pitkin Limestone and Fayetteville Shale were deposited in a marine environment in the roughly, present day east-west trending Arkoma Basin. The Arkoma Basin is bound to the north by the Ozark Dome and to the south by the Ouachita Mountains (Houseknecht, 1986). The Fayetteville Shale is made up of three members, including, in ascending order: the lower Fayetteville, the Wedington Sandstone, and the upper Fayetteville. The Fayetteville Shale fits comfortably beneath the Pitkin Limestone and represents a third-order regressive cycle, where the maximum flooding surface is represented by the lower Fayetteville Shale, followed by a transgression event leading to the deposition of the deltaic Wedington Sandstone, and followed by subsequent sea-level rise leading to the deposition of the upper Fayetteville and Pitkin Limestone (McGilvery et al., 2016).

1.3 CORE DESCRIPTION

The Nixon B #1-7 well includes the base of the Pitkin Limestone, a medium-light gray Argillaceous mudstone to wackestone with some interbedded layers of shale, and the Fayetteville Shale that is made up of three members (upper Fayetteville, Wedington Sandstone, and lower Fayetteville). In ascending order:

- The lower Fayetteville (core depths; 3,200–3,309 ft) is made up of clay-rich and fossiliferous calcareous shale with interspersed phosphorus nodules within the calcareous shale facies

- The Wedington Sandstone (cores depths; 3,120–3,135 ft) is a light gray tight sublitarenite to quartzarentite sandstone with some thinly bedded shale intervals
- The upper Fayetteville is a dark gray shale with some interbedded medium-light gray mudstone intervals.

1.4 CORE PHOTOGRAPHS

Figures 1 through 9 show photographs of the 1/3 slabbed core. Each photographed box holds up to 10 ft of core.

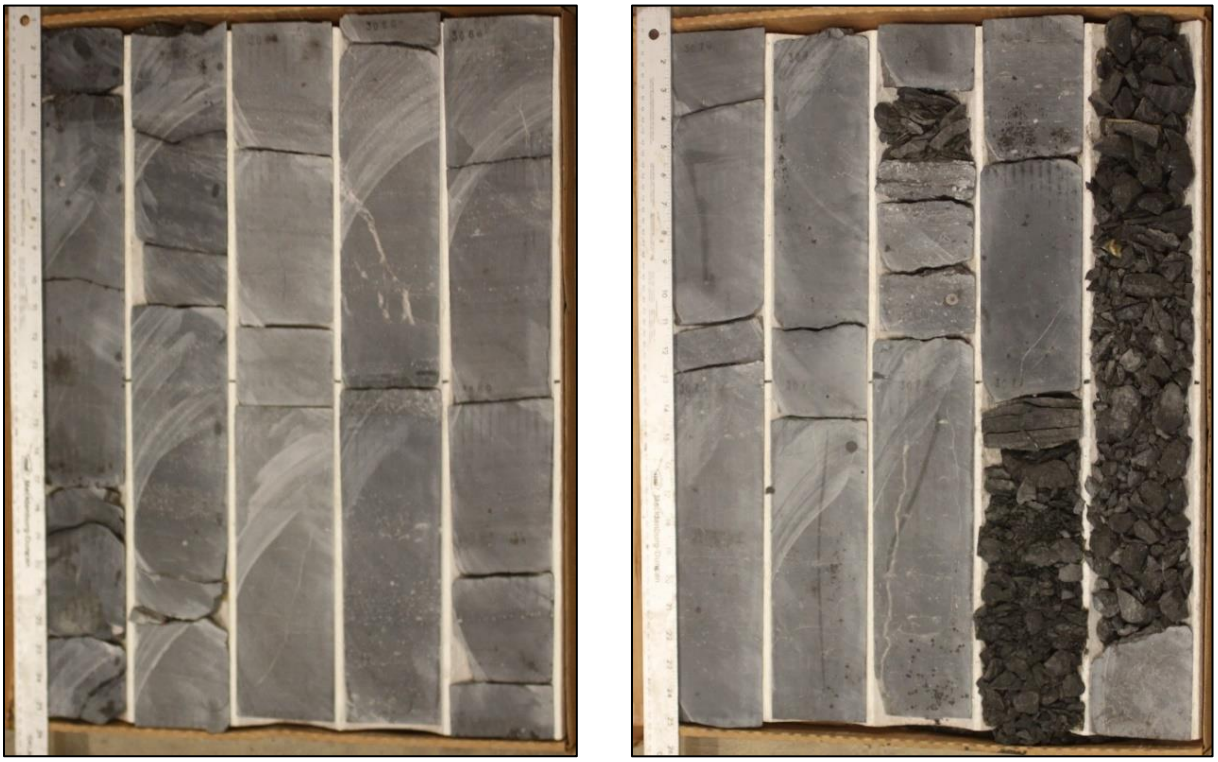

Figure 1: Photographs of Nixon B well from slabbed 3,060 to 3,080 ft.

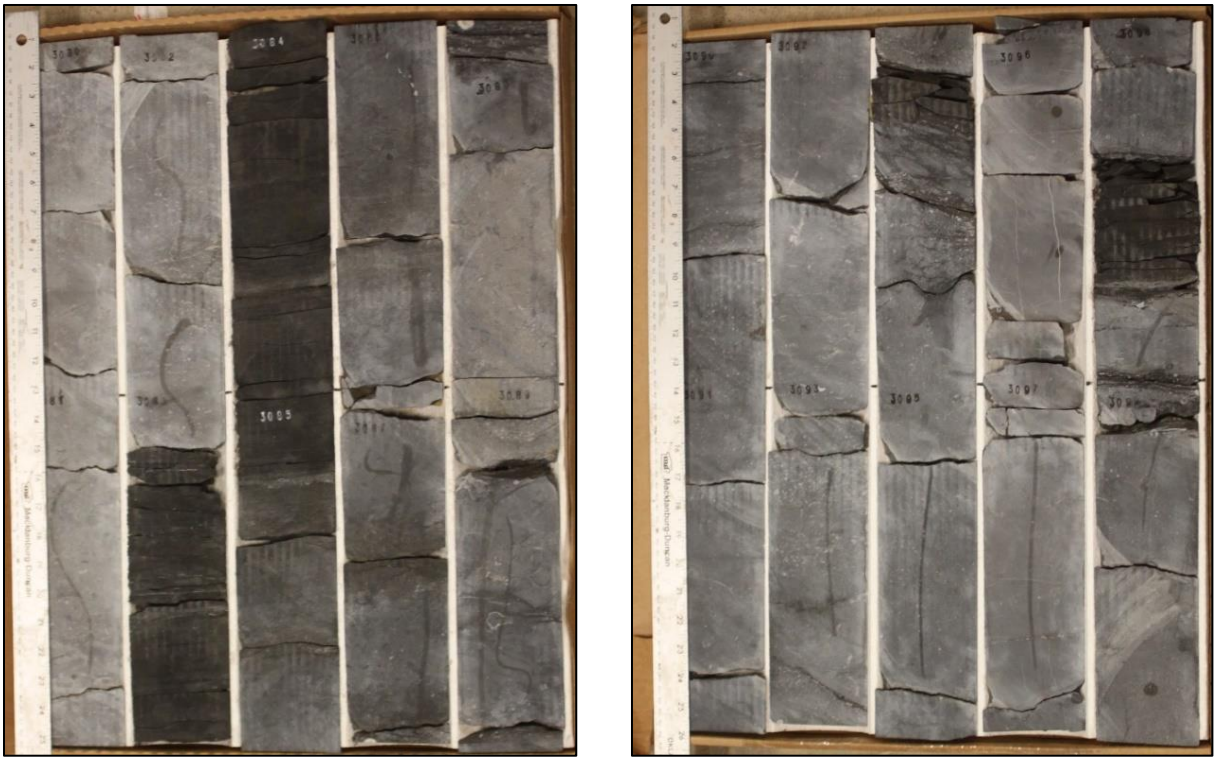

Figure 2: Photographs of Nixon B well from slabbed 3,080 to 3,100 ft.

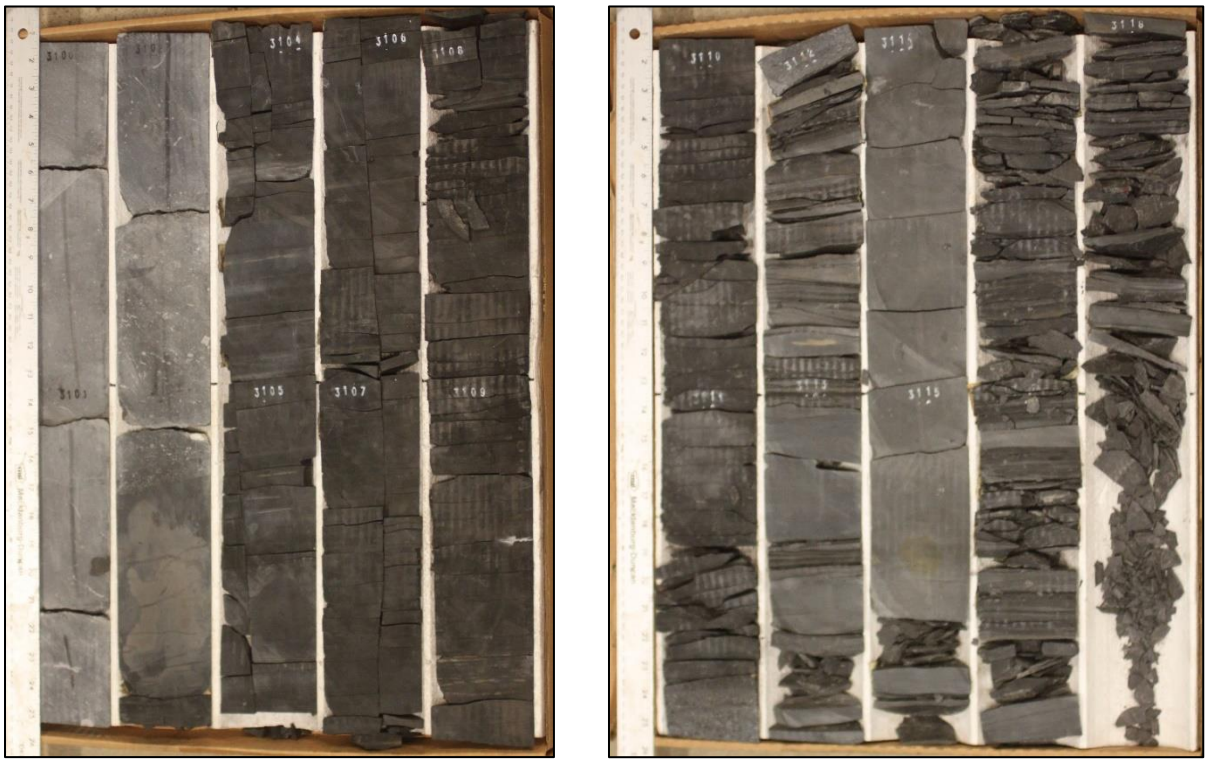

Figure 3: Photographs of Nixon B well from slabbed 3,100 to 3,120 ft.

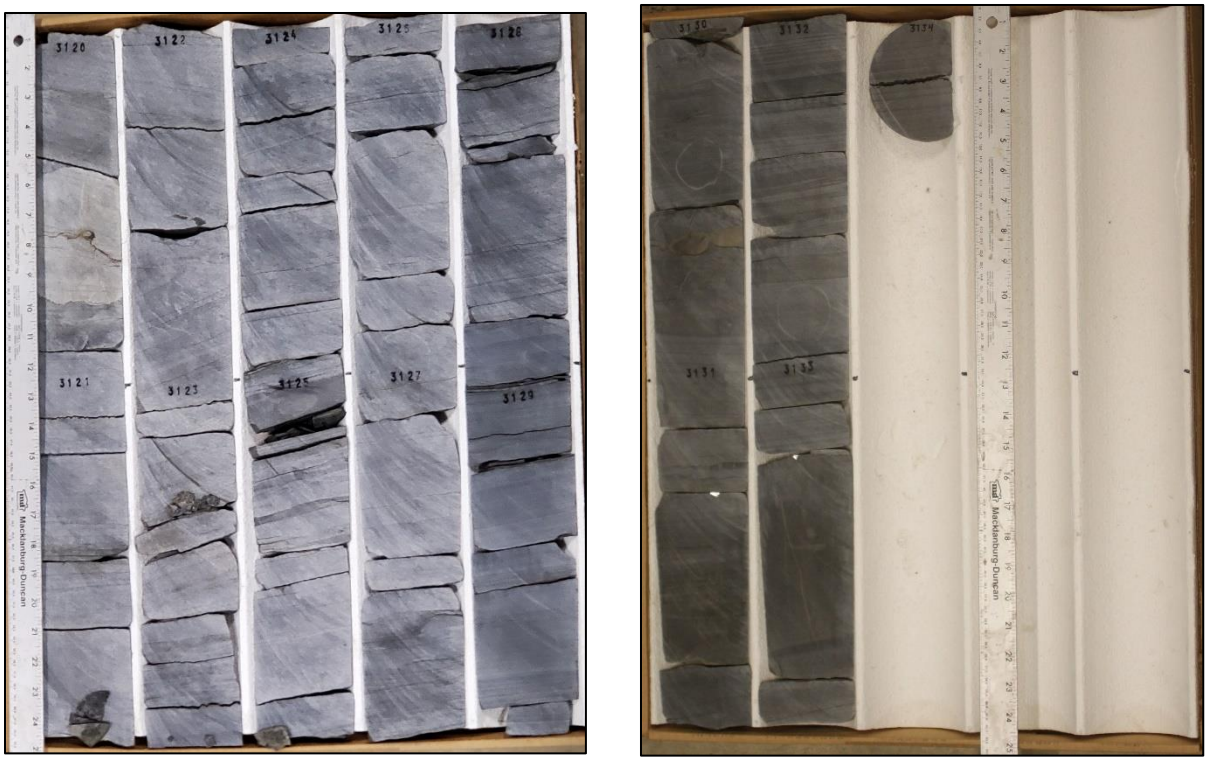

Figure 4: Photographs of Nixon B well from slabbed 3,120 to 3,134 ft.

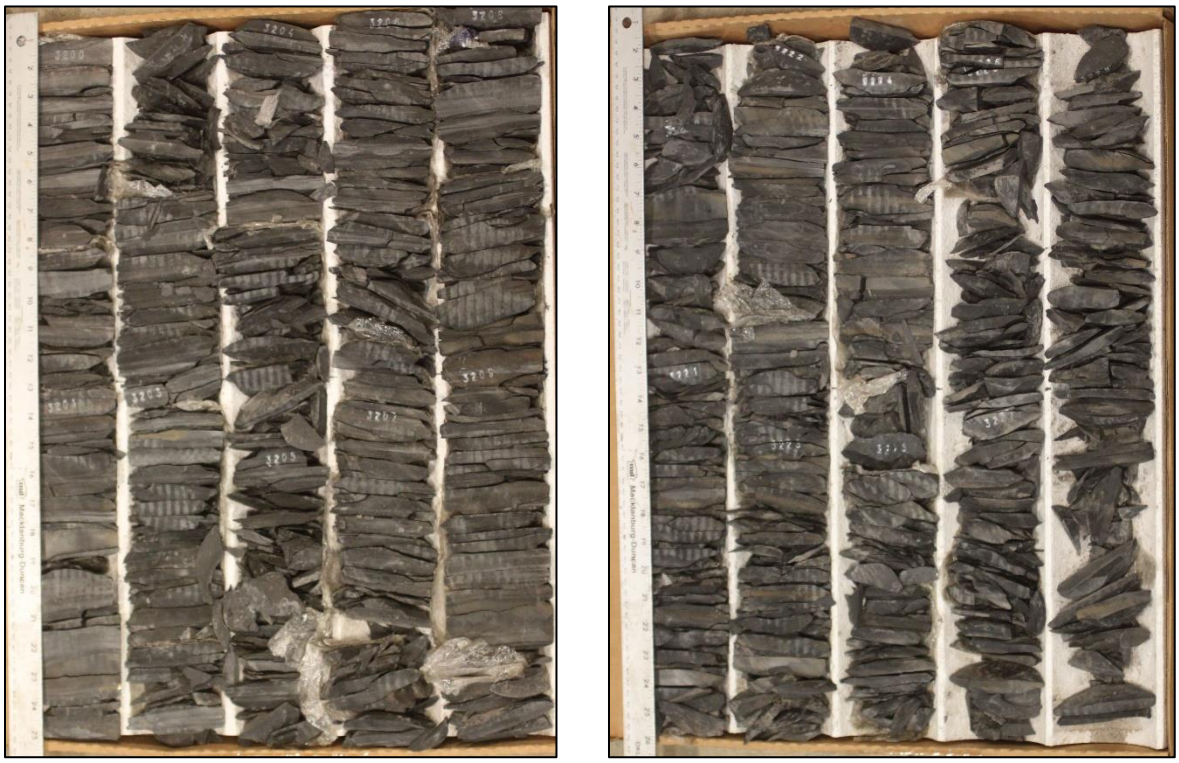

Figure 5: Photographs of Nixon B well from slabbed 3,200 to 3,220 ft.

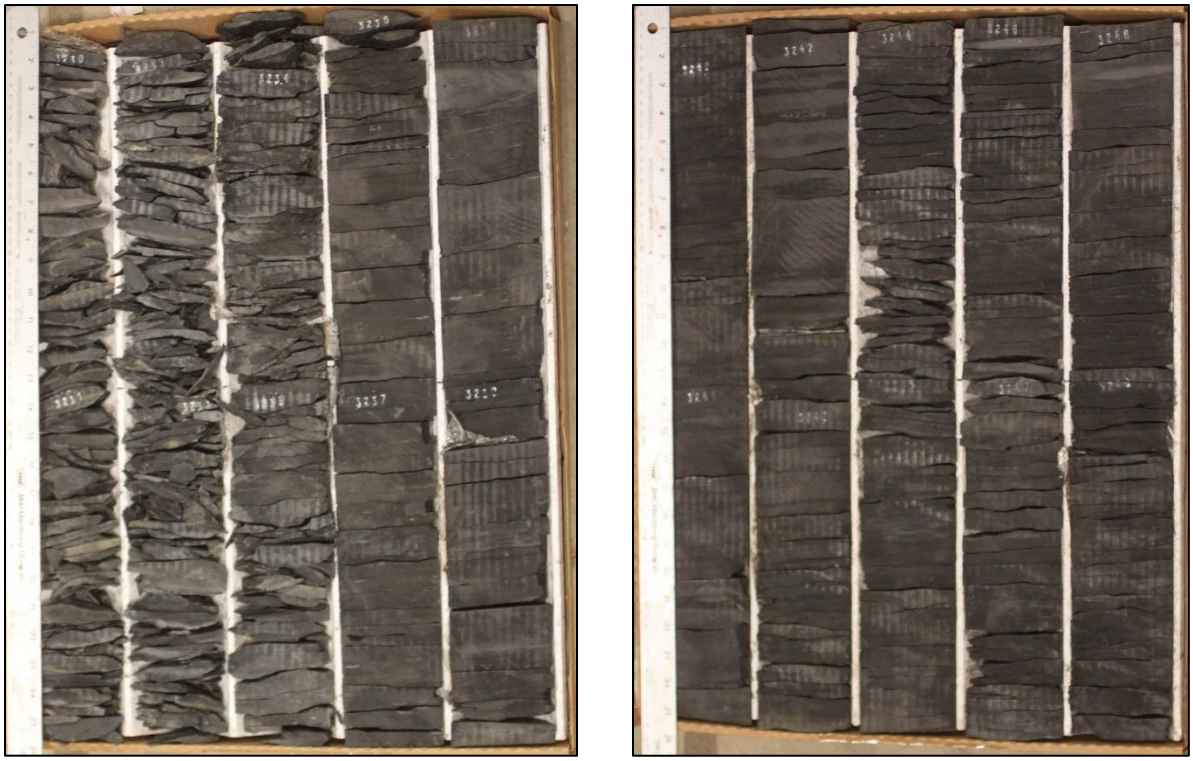

Figure 6: Photographs of Nixon B well from slabbed 3,230 to 3,250 ft.

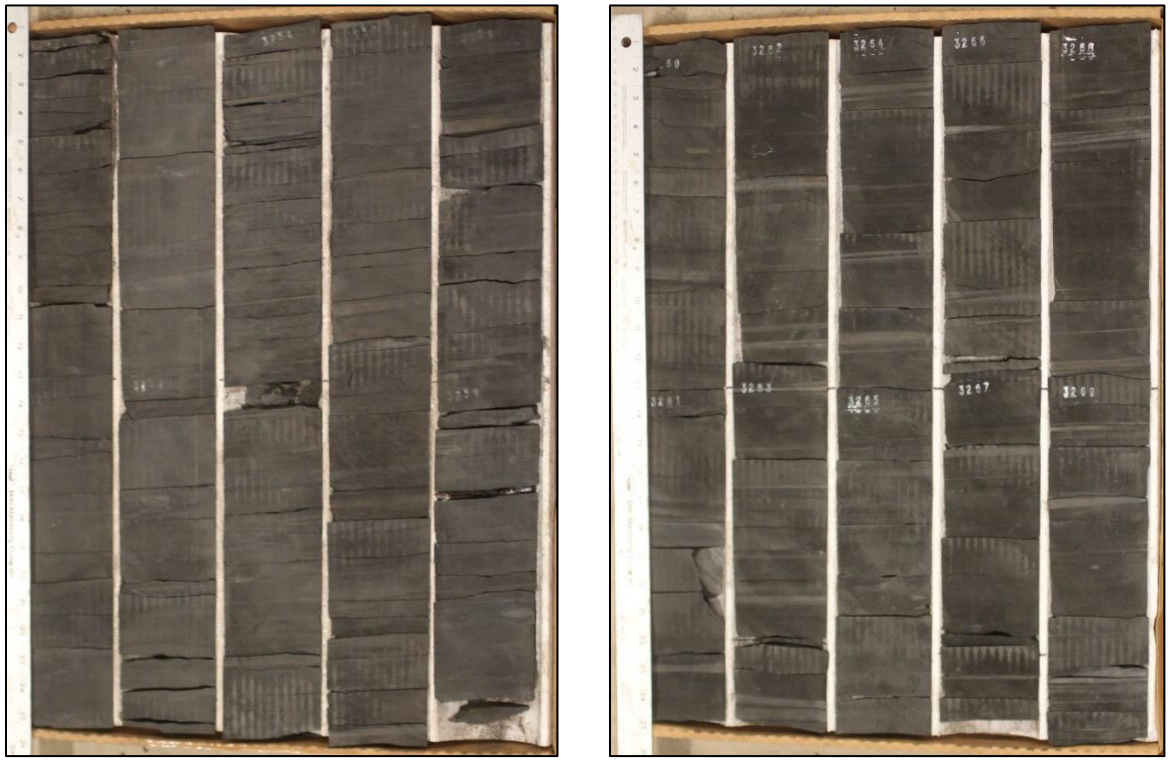

Figure 7: Photographs of Nixon B well from slabbed 3,250 to 3,270 ft.

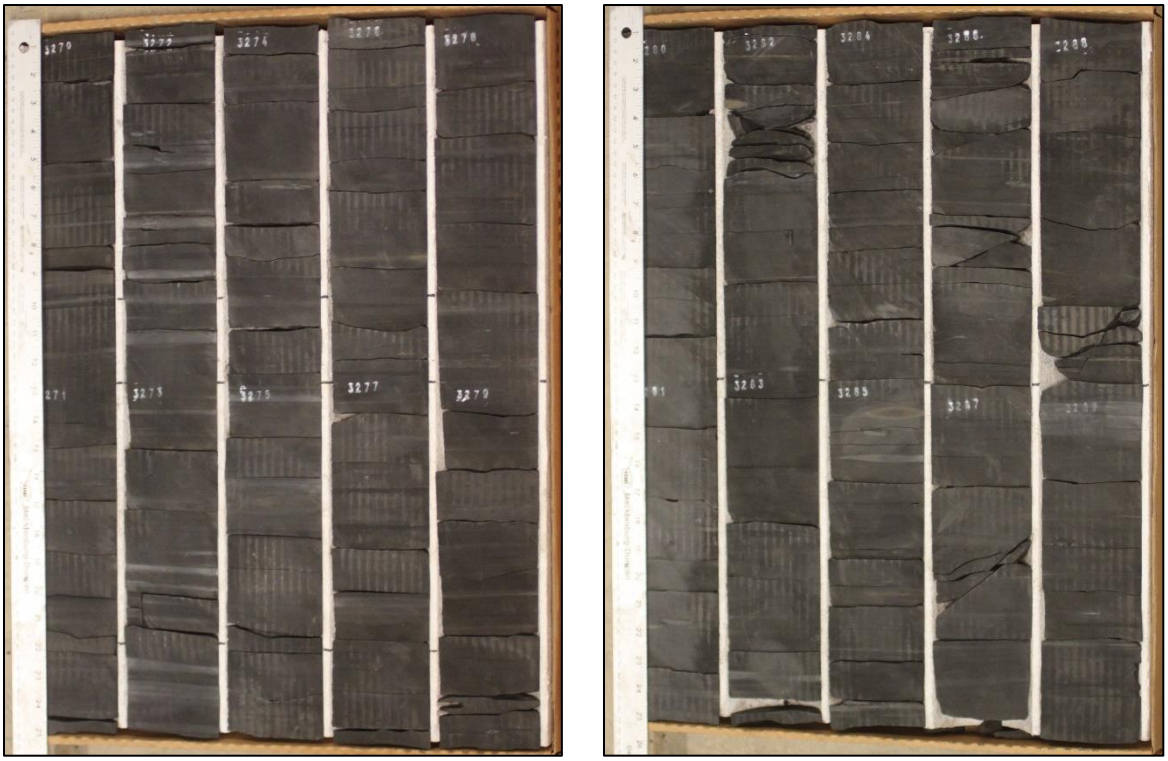

Figure 8: Photographs of Nixon B well from slabbed 3,270 to 3,290 ft.

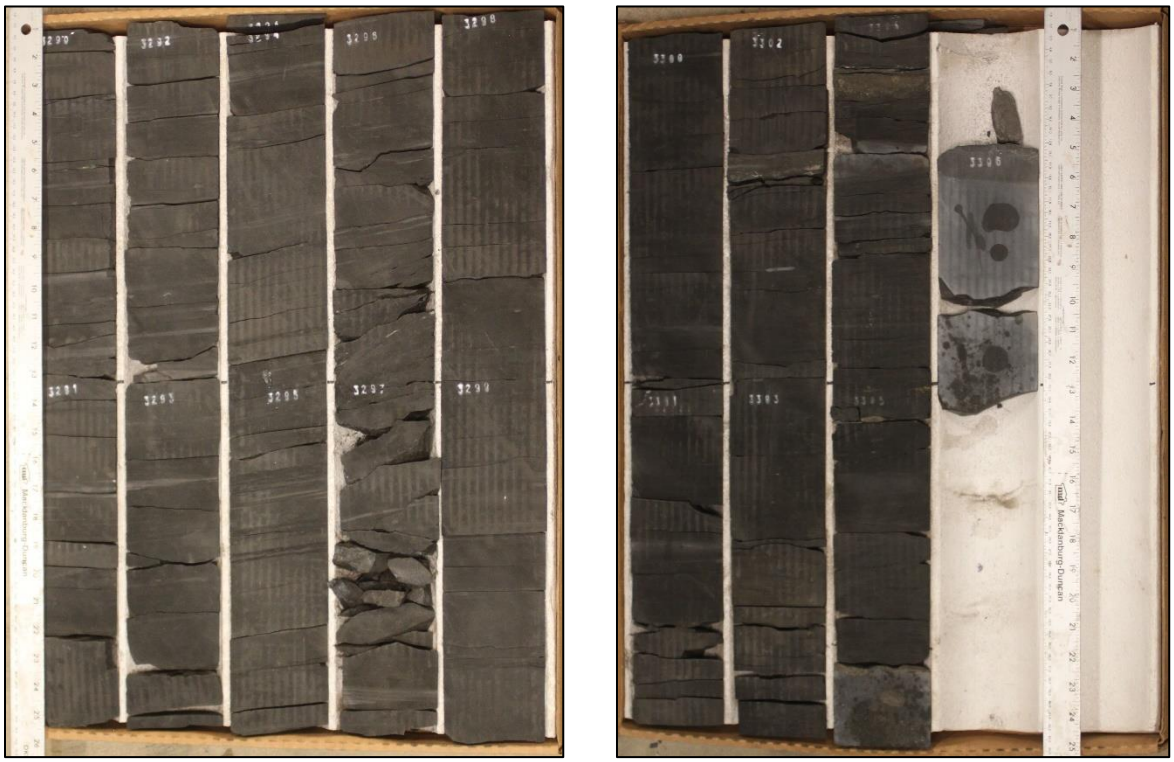

Figure 9: Photographs of Nixon B well from slabbed 3,290 to 3,307 ft.

2. DATA ACQUISITION AND METHODOLOGY

The 2/3rd slabbed core was evaluated using computed tomography (CT) scanning and traditional core logging.

2.1 CORE LOGGING

Geophysical measurements of core thickness deviation, P-wave travel time, magnetic susceptibility, and attenuated gamma counts were obtained with a Geotek® Multi-Sensor Core Logging (MSCL). Geotek® MSCL software was used to process the raw data into core thickness, P-wave velocity, gamma density, and fractional porosity values. Additionally, the system was used to measure bulk elemental chemistry with a built-in, portable X-ray fluorescence (XRF) spectrometer. The Geotek® MSCL system at the NETL has many additional capabilities (Crandall et al., 2017); however, only those that were significant to this characterization are described in the following sections (Figure 10).

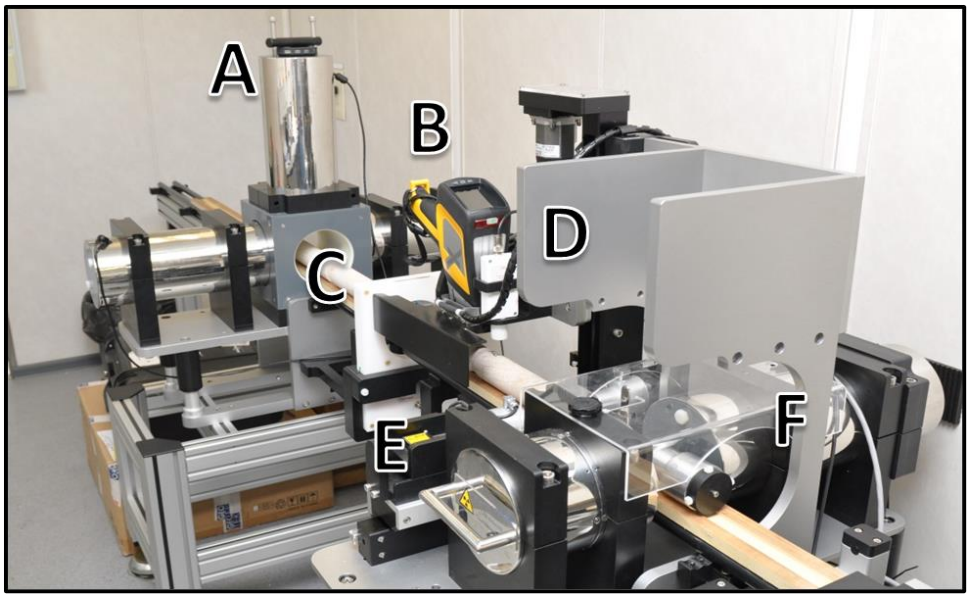

Figure 10: MSCL allows researchers to continuously run petrophysical measurements on whole core: (A) natural gamma detector; (B) XRF spectrometry sensor; (C) magnetic susceptibility loop sensor; (D) magnetic susceptibility point sensor; (E) P-wave velocity transducers; (F) gamma density source, and non-contacting electrical resistivity sensor (not shown)..

2.1.1 Magnetic Susceptibility

Magnetic susceptibility is a measure of the degree of magnetization in a sample. The sample is exposed to an external magnetic field and magnetic susceptibility is the measured magnetic response to that field:

$$J = kH$$

Where, *J* is the magnetic response (per unit volume), *k* is volume susceptibility, and *H* is an external magnetic field. The measurement unit is dimensionless (abbreviated simply as SI).

All materials have magnetic susceptibility. Positive values of magnetic susceptibility indicate that materials are paramagnetic and occur in rocks that consist of the majority ferromagnetic, ferrimagnetic, or antimagnetic (iron bearing) materials. Whereas negative values of magnetic susceptibility indicate that materials are diamagnetic and occur in rocks dominated by non-iron material (i.e., calcite or quartz). Table 1 lists examples of common magnetic susceptibility ranges (Hunts et al., 1995).

Magnetic susceptibility was measured using the Bartington point sensor, where a 1-cm diameter, low intensity (8.0 A/m RMS), non-sensitive, alternating magnetic field (2 kHz) is generated for 10 s. To minimize any potential drift in the oscillating field the point sensor was zeroed at the beginning and end of the sample, as well as after every 5th measurement. The point sensor was limited in whole core measurements due to the small field, and additionally was temperature dependent (Geotek Ltd. Multi-Sensor Core Logger Manual, Version 05-10; Geotek Ltd., 2010).

Table 1: Magnetic Susceptibility Values for Common Minerals (Hunts et al., 1995)

Mineral	x (*10^{-6}) SI
Water	9
Calcite	-7.5 to -39
Halite, Gypsum	-10 to -60
Shale	63 to 18,600
Illite, Montmorillonite	330 to 410
Pyrite	5 to 3,500
Chalcopyrite	23 to 400
Hematite	500 to 40,000
Magnetite	1,000,000 to 5,700,000

2.1.2 P-wave Velocity

P-wave velocity measurements were performed to measure the acoustic impedance of a geologic sample with compressional waves. Acoustic impedance is a measure of how well a material transmits vibrations, which is directly proportional to density and/or material consolidation. An example of a material that has a low acoustic impedance would be air, with a wave speed of 330 m/s, whereas granite would have high acoustic impedance, with a wave speed of >5,000 m/s. These measurements can be proxies for seismic reflection coefficients and can be translated to field use when doing seismic surveys.

The software associated with the MSCL measures the travel time of the pulse with a resolution of 50 ns. The absolute accuracy of the instrument measurements is $\pm$ 3 m/s with a resolution of 1.5 m/s (Geotek Ltd. Multi-Sensor Core Logger Manual, Version 05-10; Geotek Ltd., 2010).

2.1.3 X-Ray Fluorescence Spectrometry

In addition to the geophysical measurements a portable handheld Innov-X® X-Ray Fluorescence Spectrometer was used to measure relative elemental abundances of aggregated "light elements" up to and including sodium; various heavy elements were measured individually (Figure 11). Elemental abundances are reported relative to the total elemental composition, i.e., out of 100% weight.

The XRF spectrometer measures elemental abundances by subjecting the sample to X-ray photons. The high energy of the photons displaces inner orbital electrons in the respective elements. The vacancies in the lower orbitals cause outer orbital electrons to "fall" into lower orbits to satisfy the disturbed electron configuration. The substitution into lower orbitals causes a release of a secondary X-ray photon, which has an energy associated with a specific element. These relative and element specific energy emissions can then be used to determine bulk elemental composition.

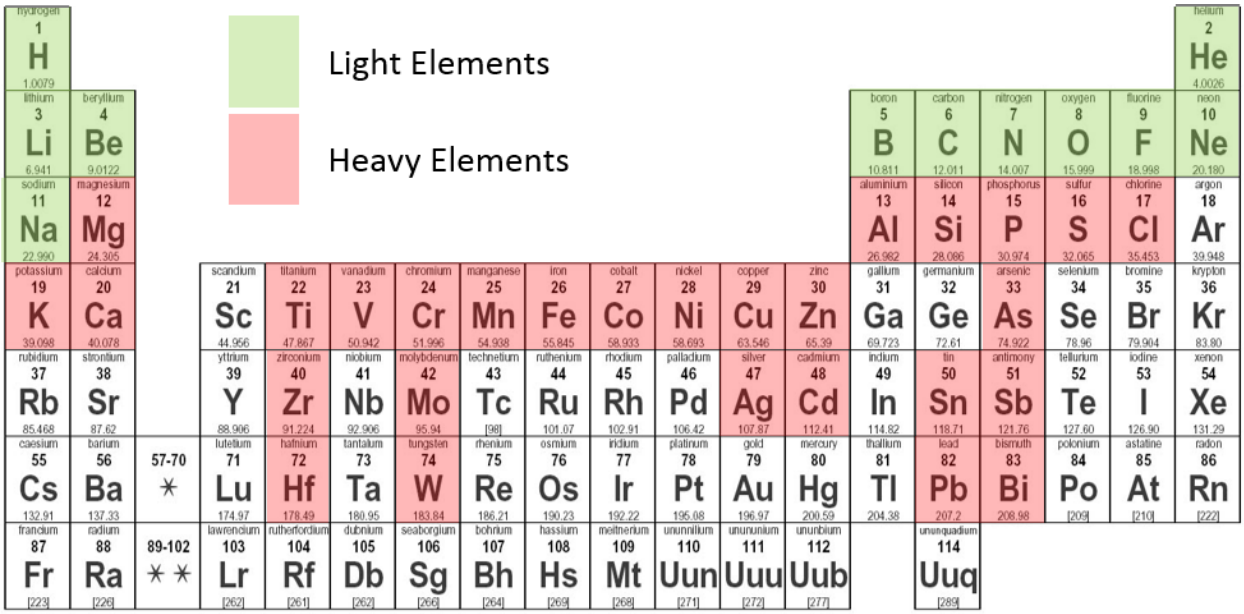

Figure 11: Periodic table showing elements measurable by the Innov-X® X-Ray Fluorescence Spectrometer (shaded).

2.2 MEDICAL CT SCANNING

Core scale CT scanning was performed with a Toshiba® Aquilion TSX-101A/R medical CT scanner as shown in Figure 12. The medical CT scanner generates images with a resolution in the millimeter range, with scans having voxel resolutions of 0.43 x 0.43 mm in the XY plane and 0.50 mm along the core axis. The scans were conducted at a voltage of 135 kV and at 200 mA. Subsequent processing and combining of stacks was performed to create three-dimensional (3D) volumetric representations of the cores and a two-dimensional (2D) cross-section through the middle of the core samples using ImageJ (Schneider et al., 2012). The variation in greyscale

values observed in the CT images indicates changes in the CT number (CTN) obtained from the CT scans, which is directly proportional to changes in the attenuation and density of the scanned rock; i.e., darker regions are less dense. As can be seen in Figures 14 through 26, filled fractures, open fractures, and changes in bedding structure can be resolved via careful examination of the CT images. While the medical CT scanner was not used for detailed characterization in this study, it allowed for non-destructive bulk characterization of the core, and thus complimented the MSCL data on the resultant logs.

Figure 12: Toshiba® Aquilion™ Multislice Helical CT Scanner at NETL used for core analysis.

2.3 MICRO-CT SCANNING

Micro-CT scanning was performed using two scanners, a ZEISS Xradia MicroXCT-400 scanner and a Tescan DynaTOM scanner. The Xradia system has the highest resolution of the scanners at NETL and scans samples sized from sub-mm to 25 mm. Tescan DynaTOM micro-CT scanner preforms both dynamic and static images and has the ability to scan both sub-mm to cm-scale samples. Both scanners provide detailed image data that can be used to infer porosity, mineralogy, and structure.

2.4 DATA COMPILATION

Strater® by Golden Software® was used to compile the MSCL and medical CT data into a series of geophysical logs. The data used to generate these logs can be accessed from NETL's Energy Data eXchange (EDX) online system using the following link: https://edx.netl.doe.gov/dataset/nixonb-1-7.

3. RESULTS

This section shows processed 2D slices of the medical CT scans through the cores, followed by the XRF and magnetic susceptibility measurements of the core from the MSCL.

3.1 MEDICAL CT SCANS

The core from the Nixon B well was scanned with a Toshiba Aquilion TSX-101A/R medical CT scanner at a sub-millimeter core-scale resolution (430 µm by 430 µm by 500 µm). As was discussed previously, the variation in greyscale values observed in the medical CT images indicates changes in the CTN obtained, which is directly proportional to changes in the attenuation and density of the scanned rock (darker regions are less dense). Core was scanned in 3 ft or smaller sections obtained from each core box. In the following images, the overall depth for each scanned sub-section of core is listed and many interesting features can readily be seen, including pyrite nodules, defined fracture planes, and fine scale layering.

3.1.1 XZ Planes

A 2D image through the center of each 3D volume can be found in Figures 14 through 26. These are referred to as "XZ" planes with the coordinates that are shown in Figure 13. The scale bar shown in these images is 2 cm; the retrieved core has a diameter of 4 in. (10.16 cm) for reference. The greyscale values were shifted in these images to best represent the structure of the core but were kept consistent across all the images.

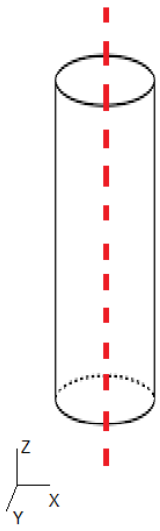

Figure 13: Schematic of the XZ isolated plane through the vertical center of the medical CT scans.

3.2 NIXON B

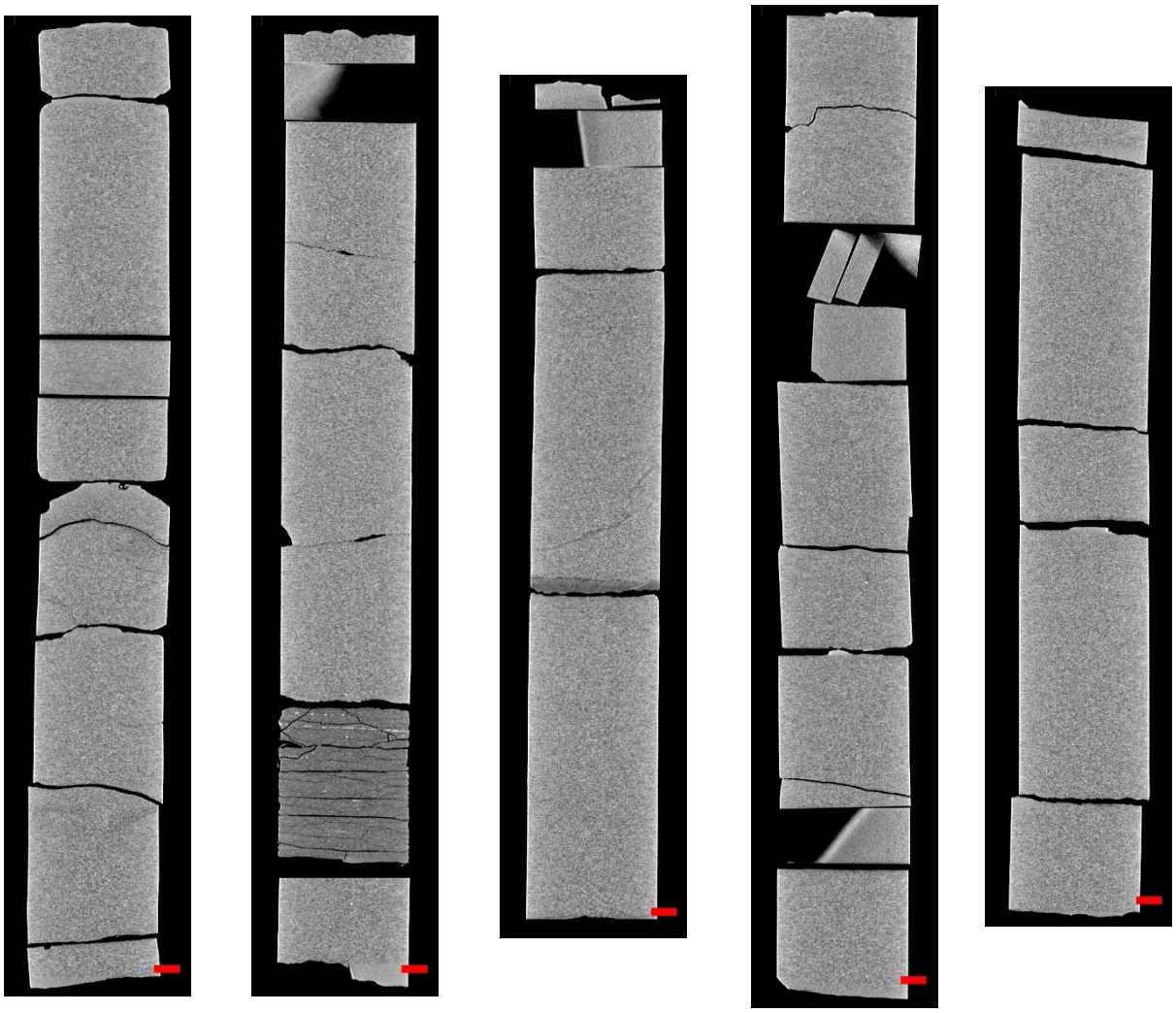

3,060–3,062.8 ft **3,062.8–3,065.5 ft** **3,065.5–3,068 ft** **3,068–3,071 ft** **3,071–3,073.2 ft**

Figure 14: 2D isolated planes through the vertical center of the medical CT scans of the Nixon B #1-7 well from 3,060 to 3,073.2 ft.

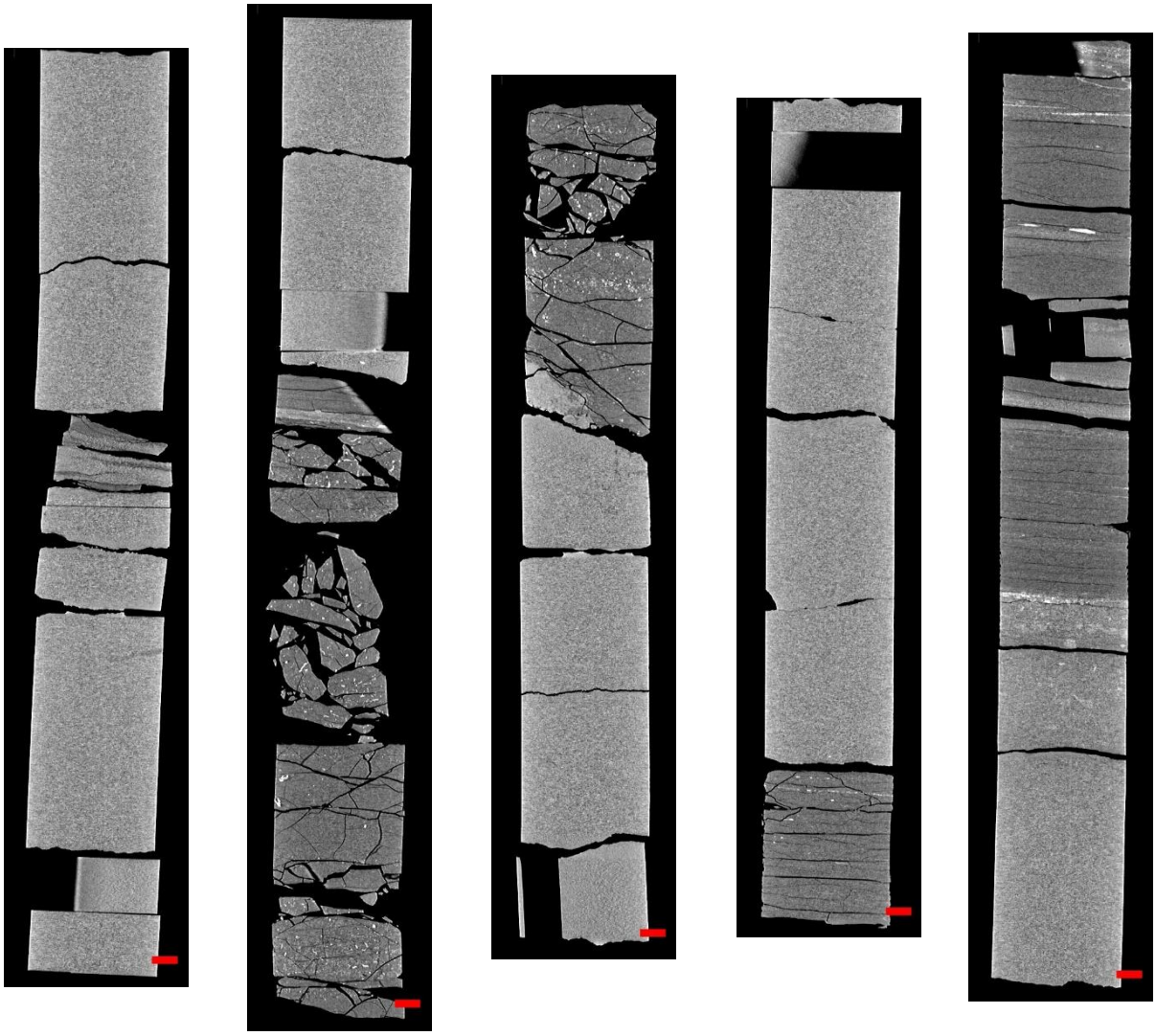

3,073.2–3,076 ft **3,076–3,078.8 ft** **3,078.8–3,081.2 ft** **3,081.2–3,083.5 ft** **3,083.5–3,086.5 ft**

Figure 15: 2D isolated planes through the vertical center of the medical CT scans of the Nixon B #1-7 well from 3,073.2 to 3,086.5 ft.

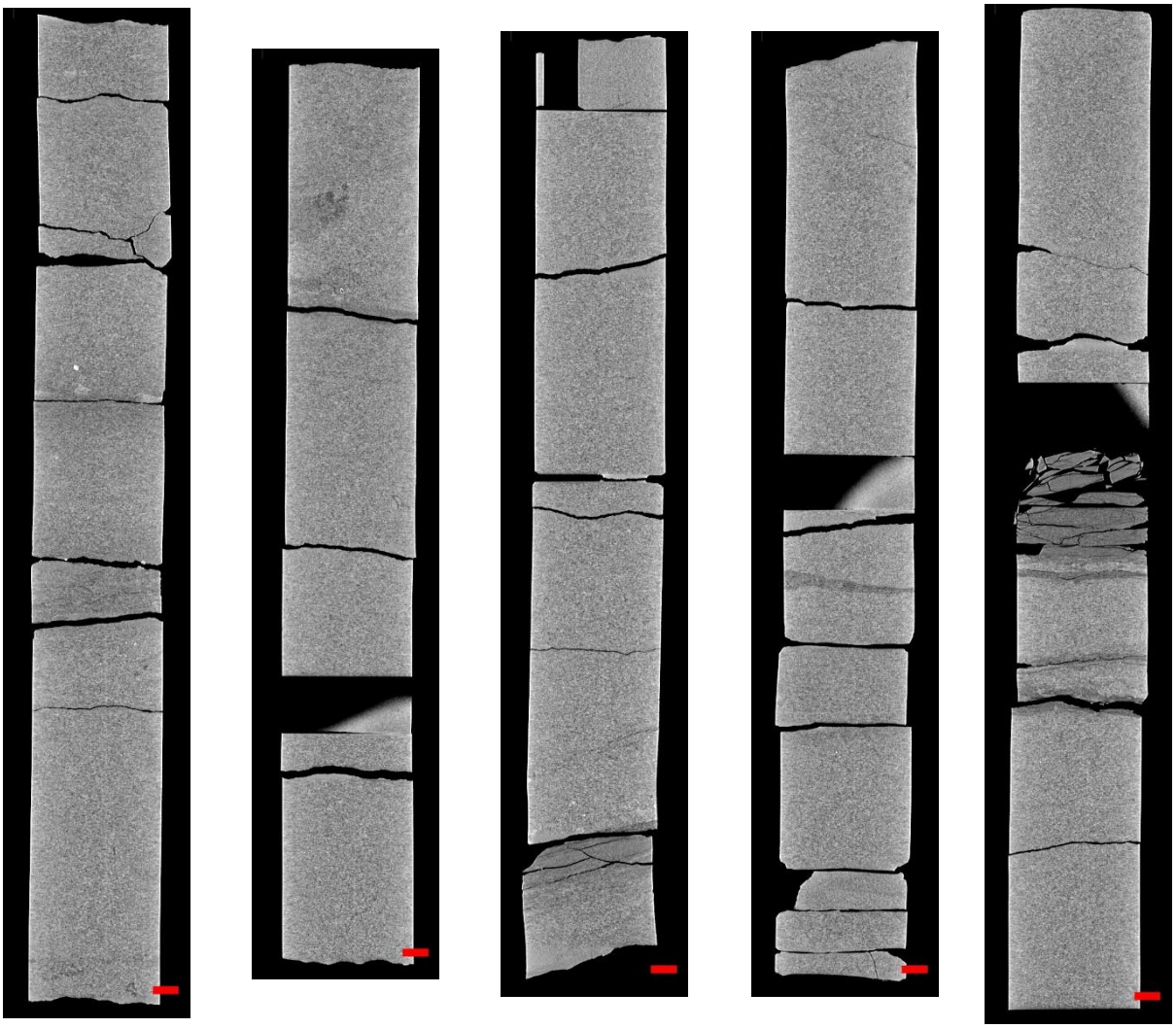

3,086.5–3,089.2 ft **3,089.2–3,091.8 ft** **3,091.8–3,094.5 ft** **3,094.5–3,097.2 ft** **3,097.2–3,100 ft**

Figure 16: 2D isolated planes through the vertical center of the medical CT scans of the Nixon B #1-7 well from 3,086.5 to 3,100 ft.

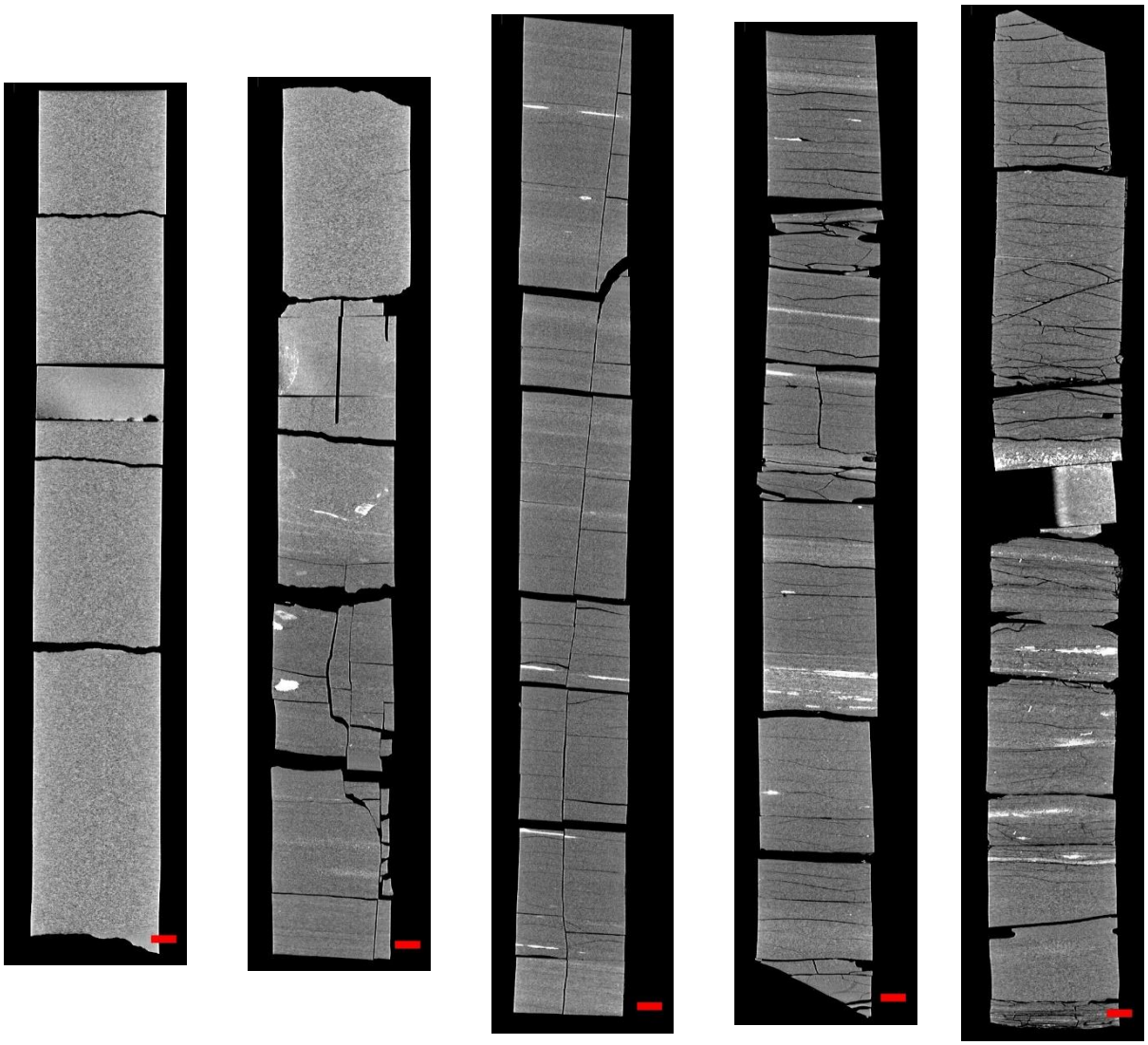

3,100–3,102.5 ft **3,102.5–3,105.6 ft** **3,105.6–3,107.7 ft** **3,107.7–3,110.6 ft** **3,110.6–3,113.6 ft**

Figure 17: 2D isolated planes through the vertical center of the medical CT scans of the Nixon B #1-7 well from 3,100 to 3,113.6 ft.

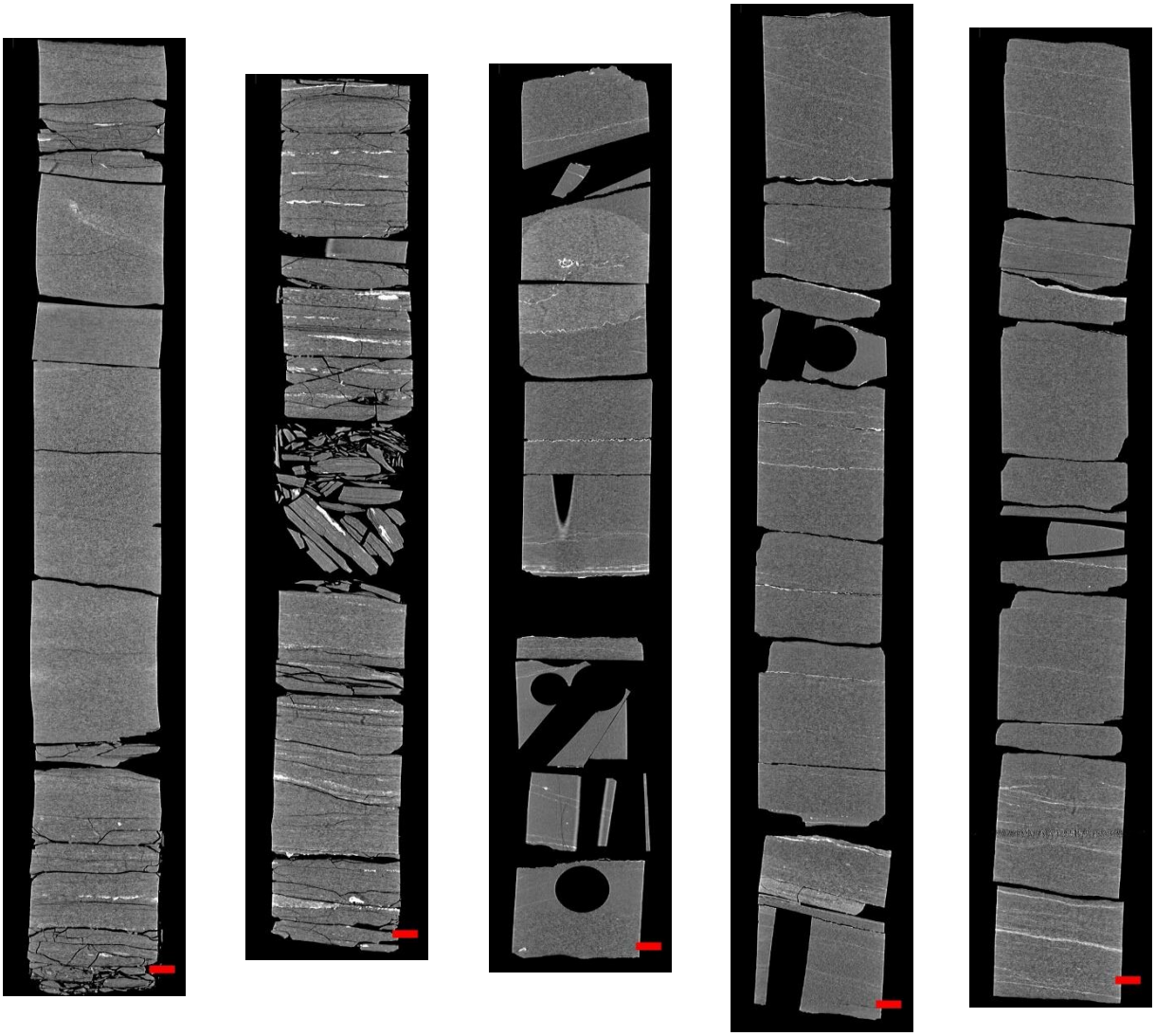

3,113.6–3,116.5 ft **3,116.5–3,120 ft** **3,120–3,122.5 ft** **3,122.5–3,125.4 ft** **3,125.4–3,128.3 ft**

Figure 18: 2D isolated planes through the vertical center of the medical CT scans of the Nixon B #1-7 well from 3,113.6 to 3,128.3 ft.

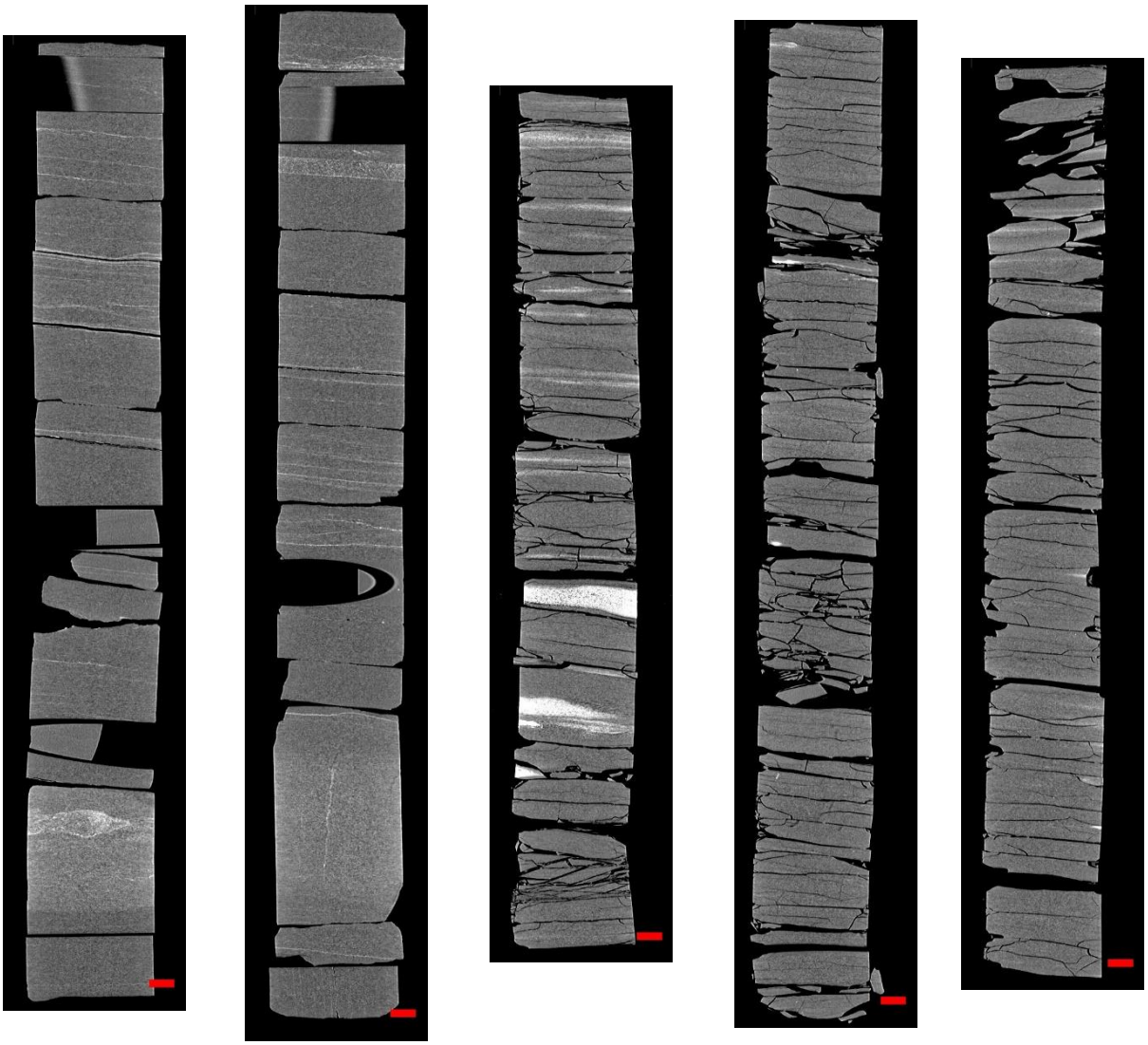

3,128.3–3,131.1 ft **3,131.1–3,134 ft** **3,200–3,202.7 ft** **3,202.7–3,205.1 ft** **3,205.1–3,208 ft**

Figure 19: 2D isolated planes through the vertical center of the medical CT scans of the Nixon B #1-7 well from 3,128.3 to 3,134 ft and 3,200 to 3,208 ft.

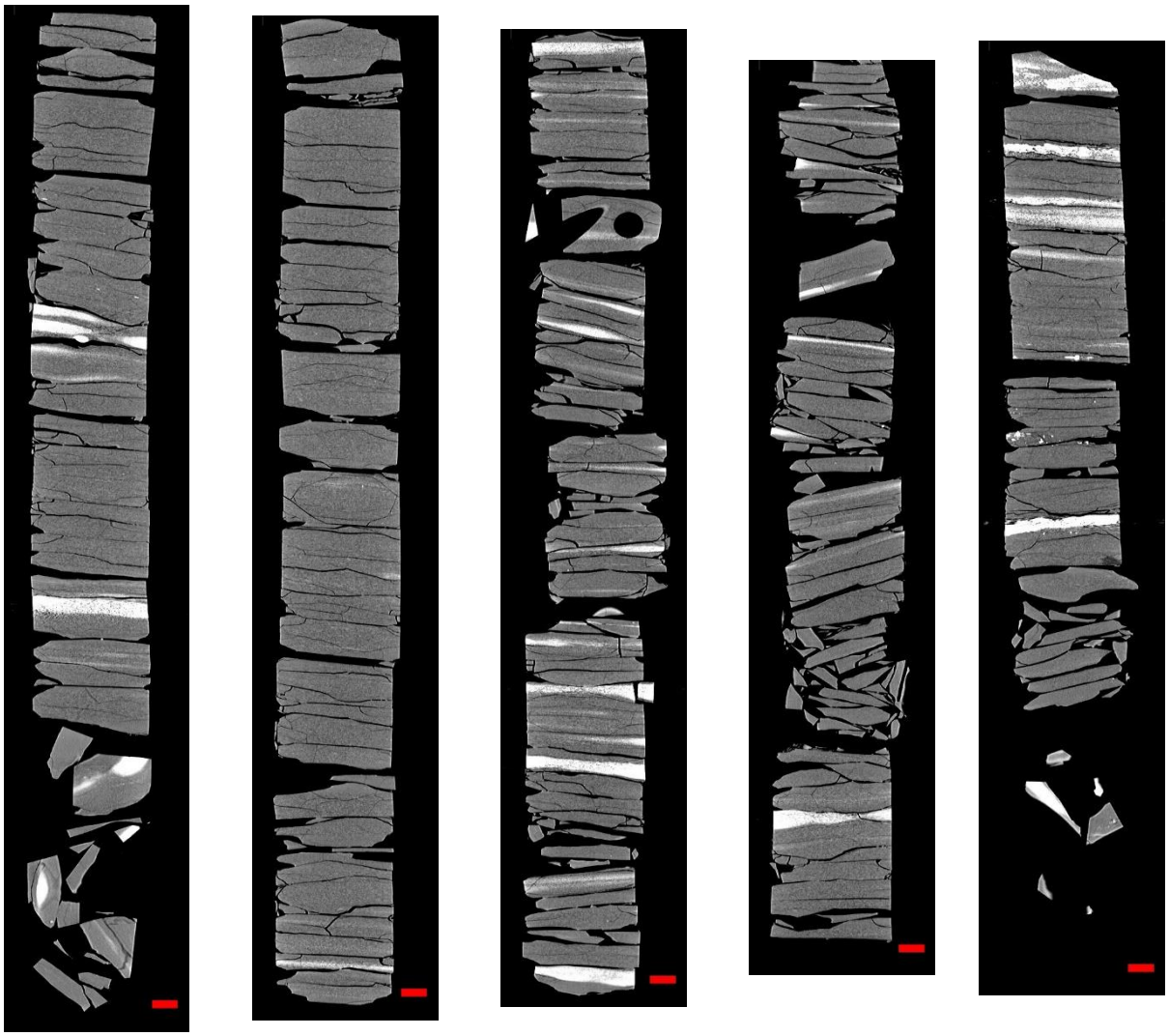

3,208–3,210.75 ft **3,210.75–3,213.6 ft** **3,213.6–3,216.1 ft** **3,216.1–3,218.5 ft** **3,218.5–3,220.7 ft**

Figure 20: 2D isolated planes through the vertical center of the medical CT scans of the Nixon B #1-7 well from 3,208 to 3,220.7 ft.

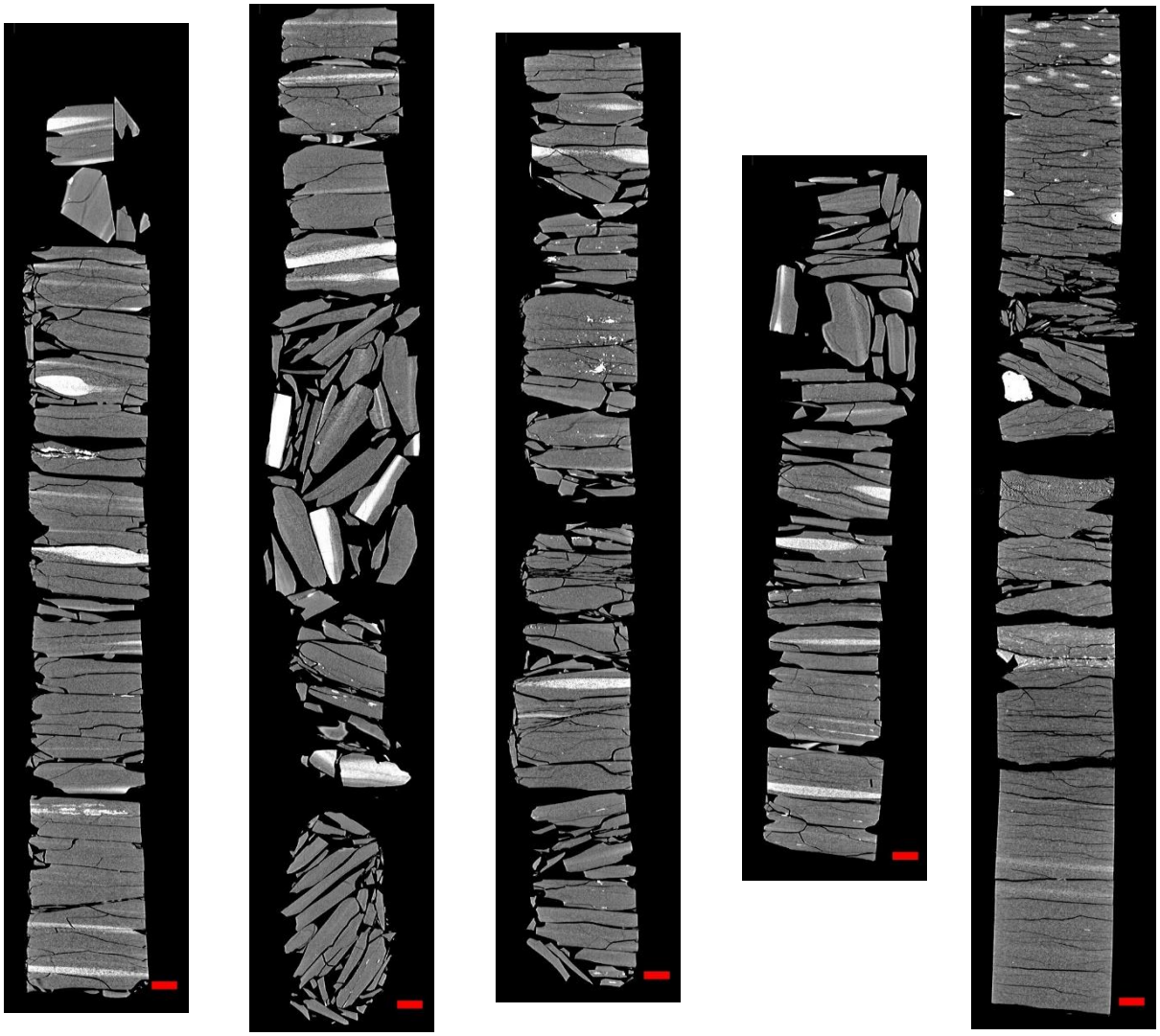

3,220.7–3,222.1 ft **3,222.1–3,225 ft** **3,225–3,228 ft** **3,228–3,231 ft** **3,234–3,237 ft**

Figure 21: 2D isolated planes through the vertical center of the medical CT scans of the Nixon B #1-7 well from 3,220.7 to 3,237 ft.

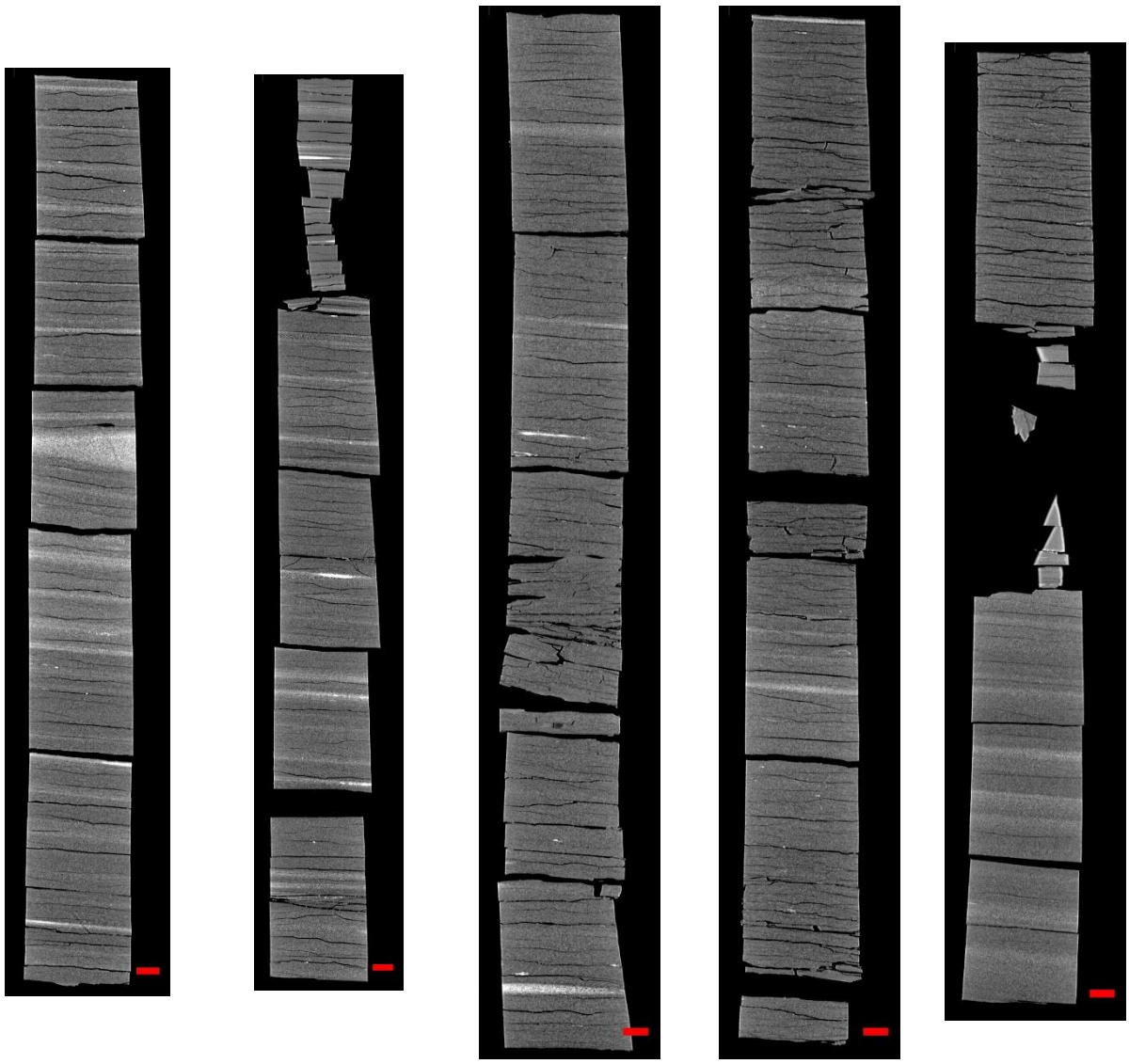

3,237–3,240 ft **3,240–3,243 ft** **3,243–3,246 ft** **3,246–3,249.2 ft** **3,249.2–3,252 ft**

Figure 22: 2D isolated planes through the vertical center of the medical CT scans of the Nixon B #1-7 well from 3,237 to 3,252 ft.

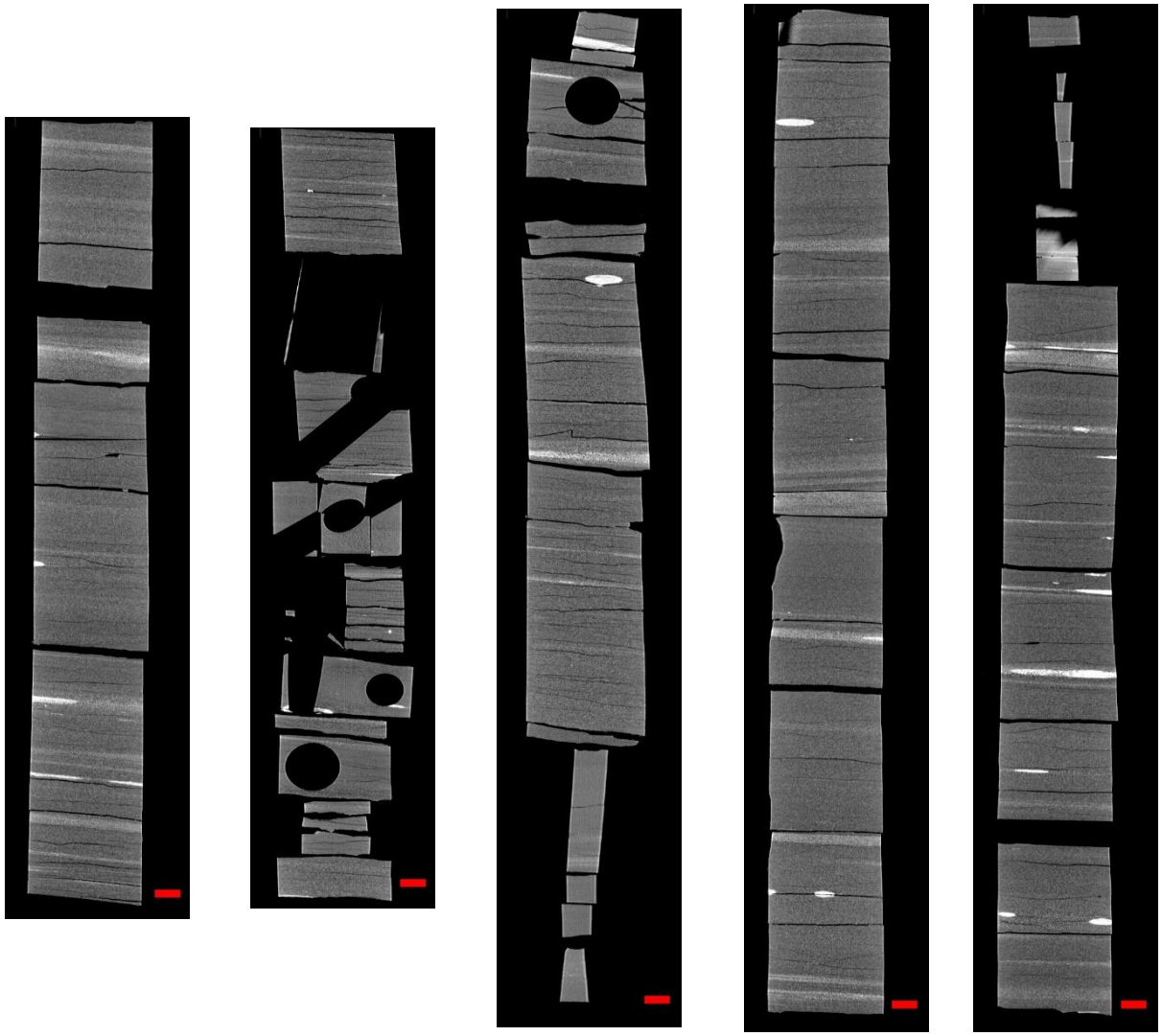

3,252–3,254.2 ft **3,254.2–3,256.9 ft** **3,256.9–3,260 ft** **3,260–3,263 ft** **3,263–3,265.9 ft**

Figure 23: 2D isolated planes through the vertical center of the medical CT scans of the Nixon B #1-7 well from 3,252 to 3,265.9 ft.

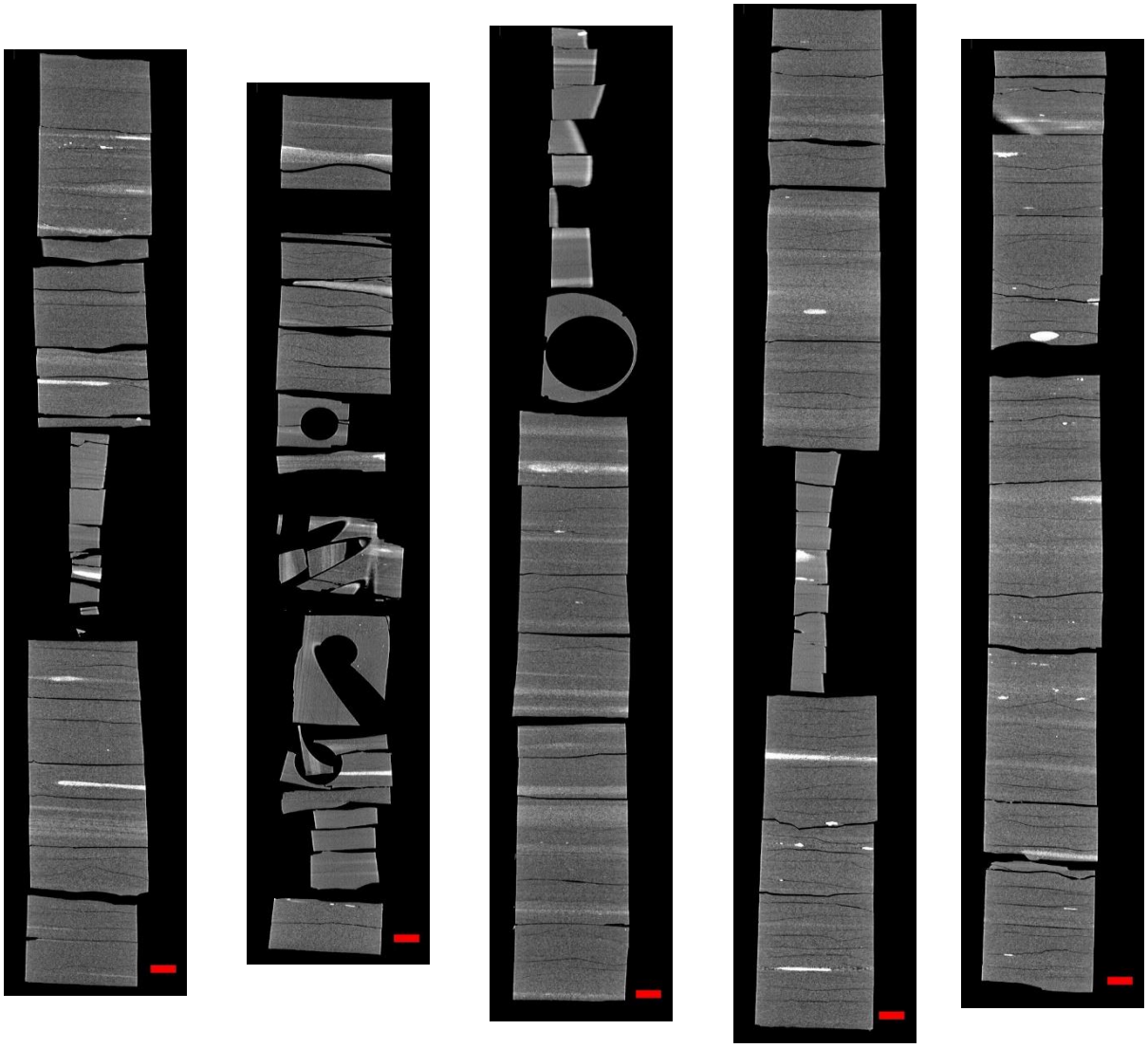

3,265.9–3,268.8 ft **3,268.8–3,271.6 ft** **3,271.6–3,274.5 ft** **3,274.5–3,277.4 ft** **3,277.4–3,280.3 ft**

Figure 24: 2D isolated planes through the vertical center of the medical CT scans of the Nixon B #1-7 well from 3,265.9 to 3,280.3 ft.

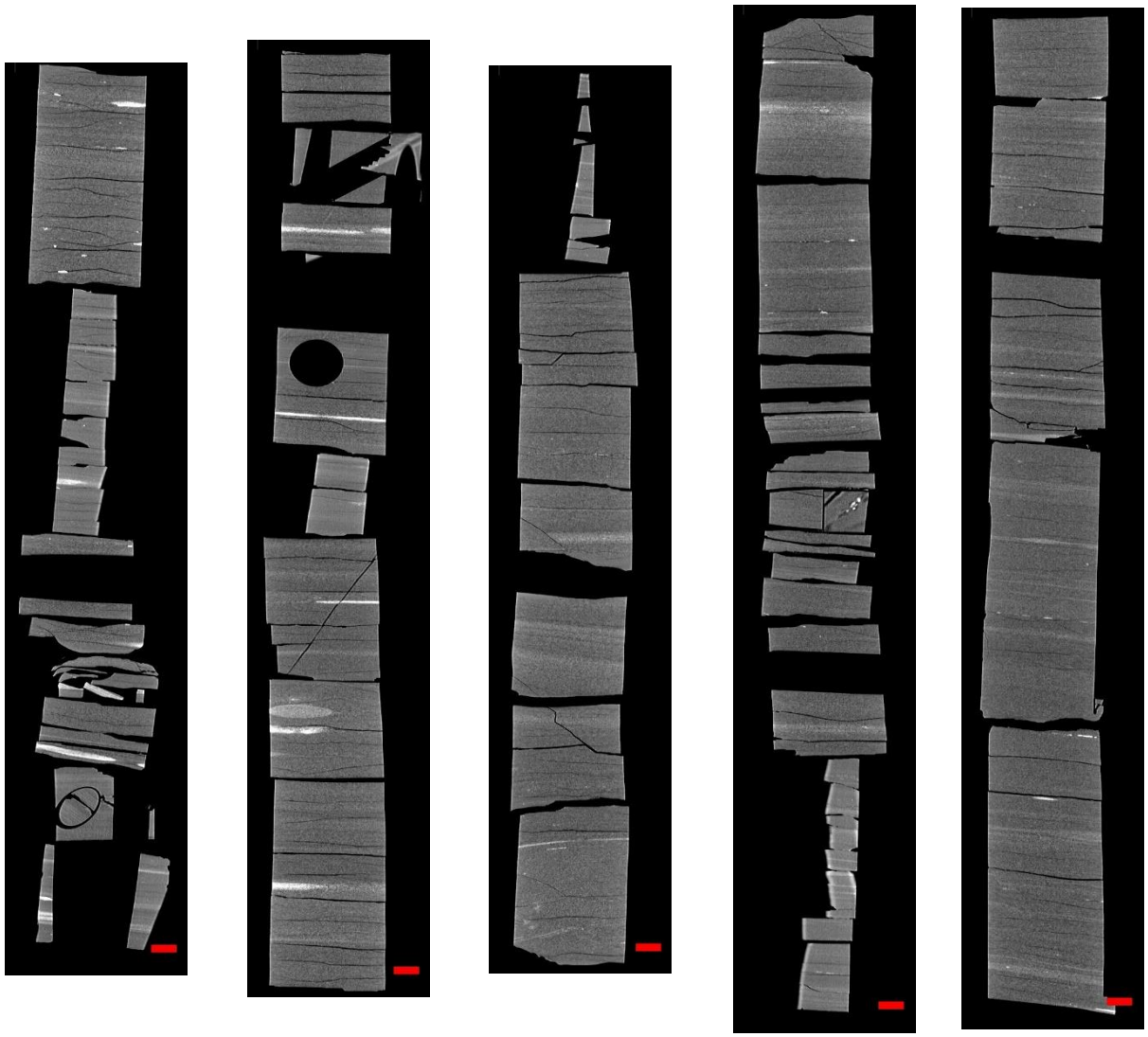

3,280.3–3,283 ft **3,283–3,286 ft** **3,286–3,288 ft** **3,288–3,291.7 ft** **3,291.7–3,294.6 ft**

Figure 25: 2D isolated planes through the vertical center of the medical CT scans of the Nixon B #1-7 well from 3,280.3 to 3,294.6 ft.

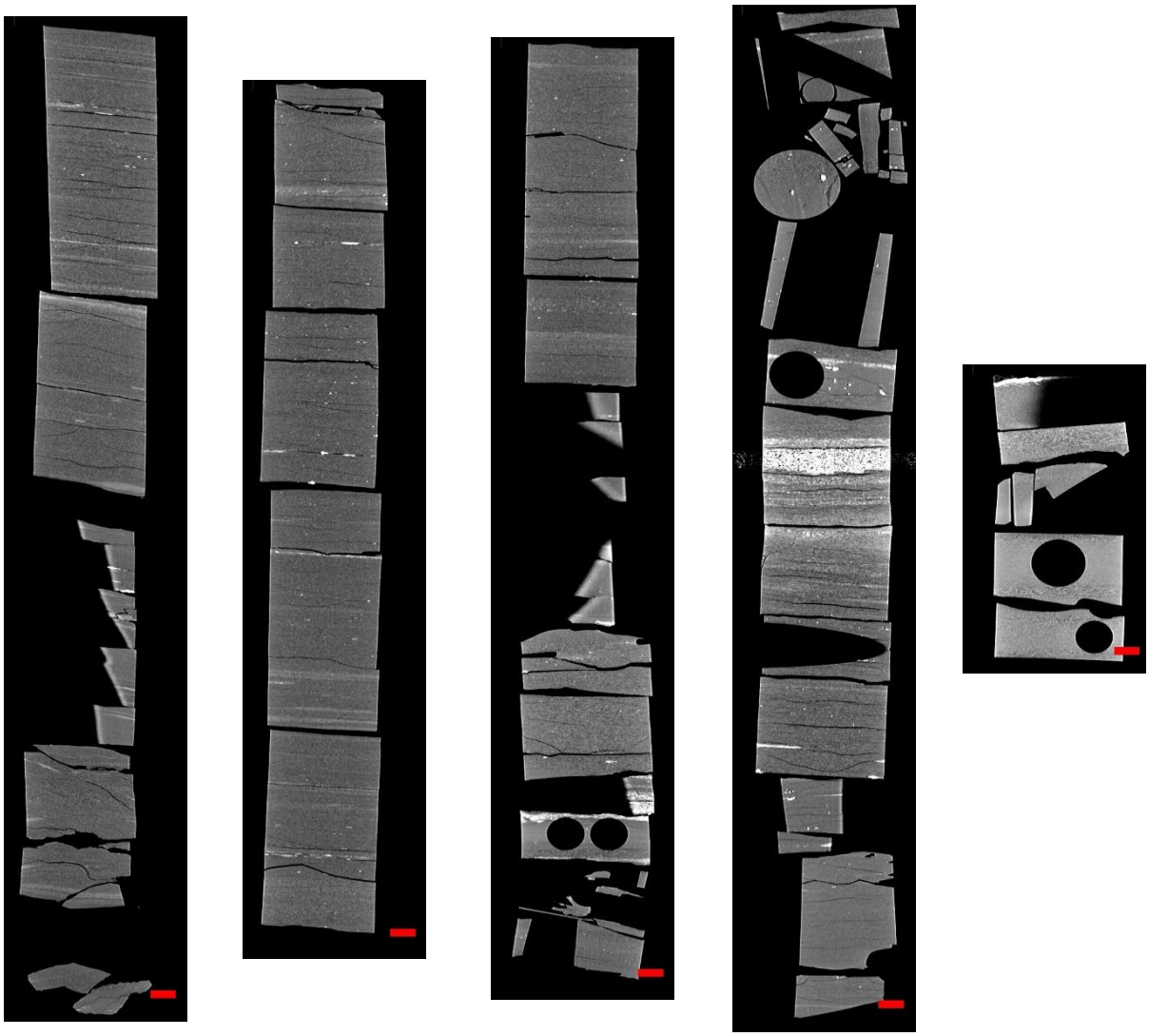

3,294.6–3,297.6 ft **3,297.6–3,300 ft** **3,300–3,304 ft** **3,304–3,305.8 ft** **3,305.8–3,307 ft**

Figure 26: 2D isolated planes through the vertical center of the medical CT scans of the Nixon B #1-7 well from 3,294.6 to 3,307 ft.

3.3 ADDITIONAL CT DATA

Additional CT data can be accessed from NETL's EDX online system using the following link: https://edx.netl.doe.gov/dataset/nixonb-1-7. The original CT data is available as 16-bit tif stacks suitable for reading with ImageJ (Schneider et al., 2012) or other image analysis software.

3.3.1 Medical CT Image Videos

In addition to the CT data, videos showing the variation along the length of the cross-section images shown in the previous section are available for download and viewing on EDX. A single image from these videos is shown in Figure 27, where the distribution of high-density minerals in a cross section of the core from a depth of 3,105.6 to 3,107.7 ft is shown. Here, the red line through the XZ-plane on the image of the core shows the location of the XY-plane displayed above (Figure 13). The videos on EDX show this XY variation along the entire length of the core.

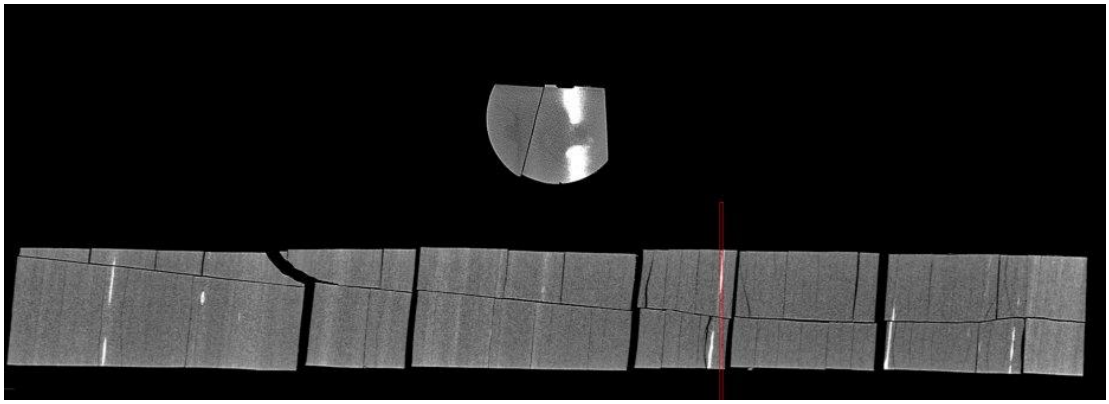

Figure 27: Single image from a video file available on EDX showing variation in the Nixon B #1-7 core from 3,105.6 to 3,107.7 ft. This shows the variation in composition within the matrix perpendicular to the core length. Note the bright (high density) concretions in the matrix.

3.3.2 Micro CT Scanning

Detailed micro CT scans of mm-scale sub-cores from select regions of Nixon B #1-7 were performed at NETL. The micro CT scanners discussed in Section 2.3 were used to obtain higher resolution images with voxel resolutions between 1.03 and 43.18 μm^3 and capture the details of internal features clearly. A list of the core sections scanned with the micro CT scanner is shown in Table 2, followed by montages of images along the length of these small core scans (Figure 28 to Figure 32).

Table 2: Micro CT Scans from Whole Core

Depth	File Name	Resolution (μm^3)
3,063.0	20210713 Nixon B 3063	2.05
3,112.0	20210813 Nixon B 3112.0 C1B20_4x	1.30
3,128.0	20220223 Nixon B 1-7 C2B3 3128.0	1.87
3,130.4	NixonB1_7_3130_4	43.2
3,130.4	NixonB1_7_3130_4closeview	20.4

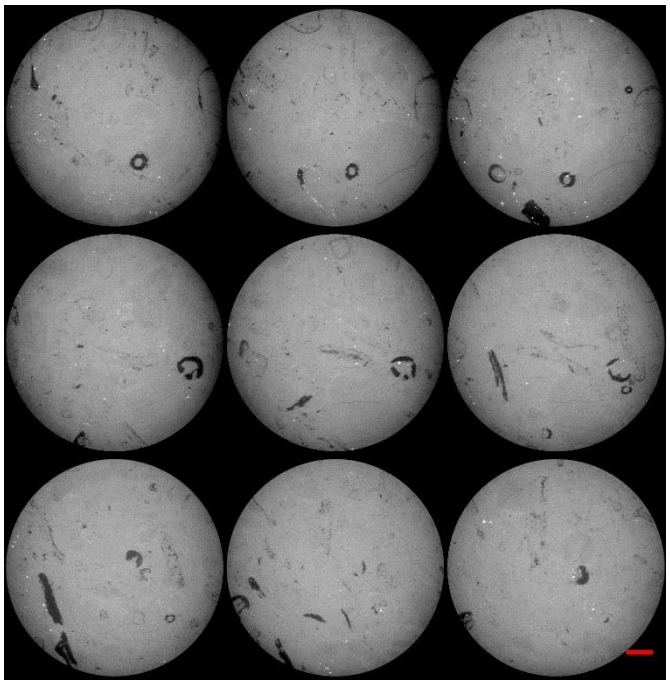

Figure 28: Micro CT montage of "20210713 Nixon B 3063"; scale bar represents 500 µm.

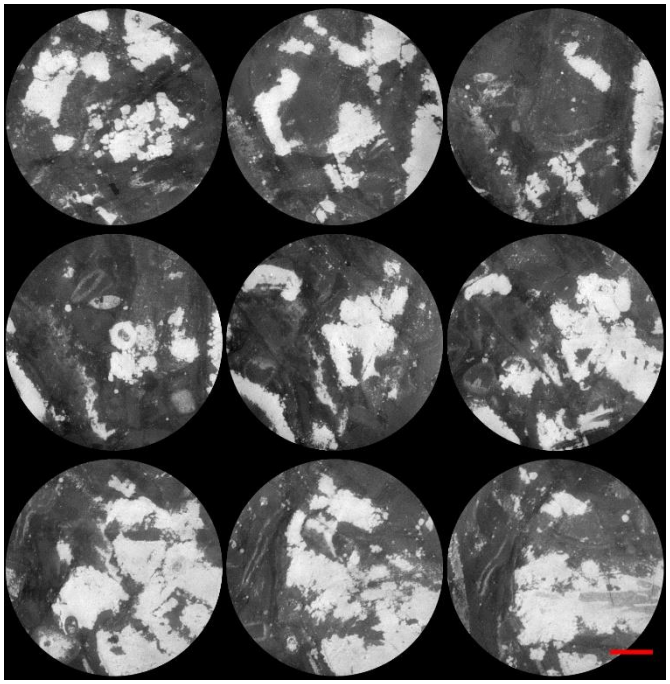

Figure 29: Micro CT montage of "20210813 Nixon B 3112.0 C1B20_4x"; scale bar represents 500 µm.

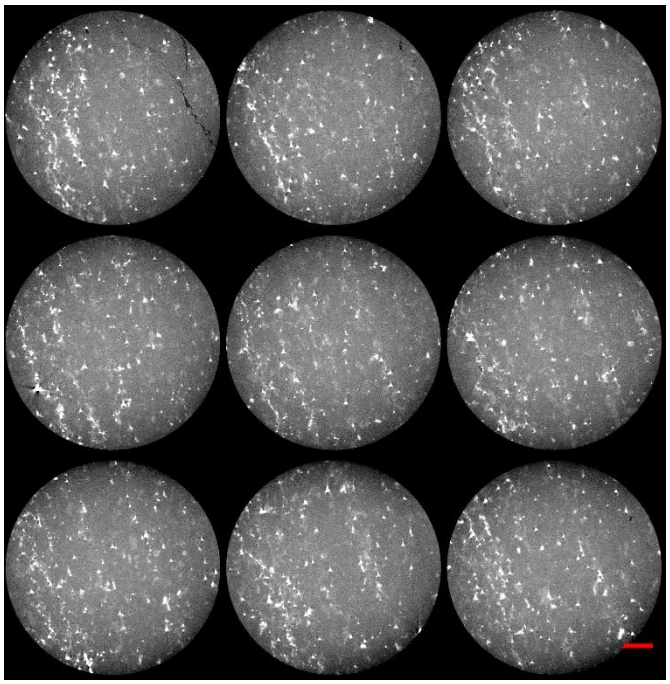

Figure 30: Micro CT montage of "20220223 Nixon B 1-7 C2B3 3128.0"; scale bar represents 500 µm.

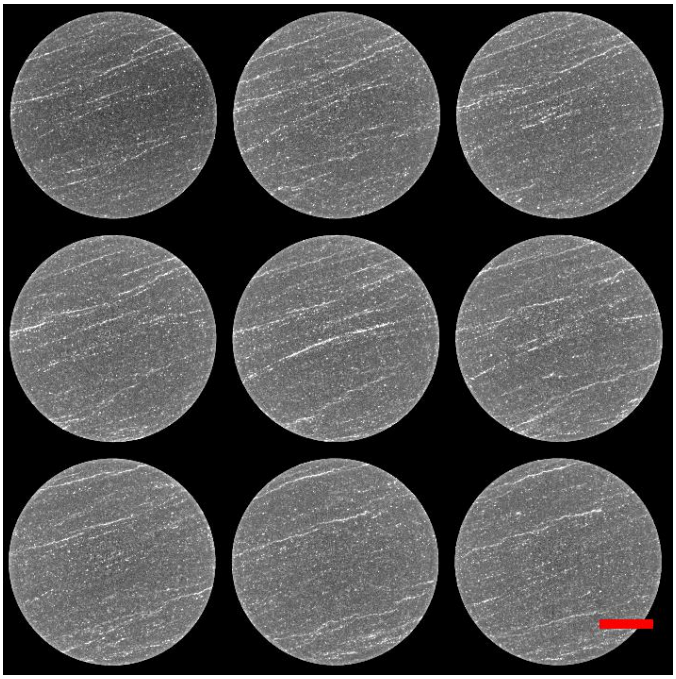

Figure 31: Micro CT montage of "NixonB1_7_3130_4"; scale bar represents 1 cm.

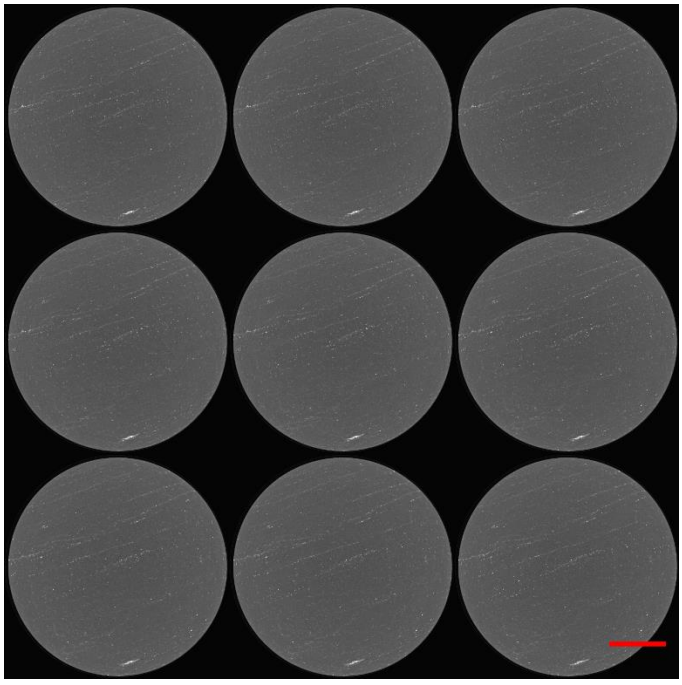

Figure 32: Micro CT montage of "NixonB1_7_3130_4closeview" ; scale bar represents 1 cm.

3.4 DUAL ENERGY CT SCANNING

Dual energy CT scanning uses two sets of images, produced at different X-ray energies, to approximate the density (ρ_B) (Siddiqui and Khamees, 2004; Johnson, 2012). This technique relies on the use of several standards of known ρ_B to be scanned at the same energies as the specimen. These scans are performed at lower energies (<100 KeV) and higher energies (>100 KeV) to induce two types of photon interactions with the object (Figure 33). The lower energy scans induce photoelectric absorption, which occurs when the energy of the photon is completely absorbed by the object mass and causes ejection of an outer orbital electron (Figure 33a). The high energy scans induce Compton scattering, which causes a secondary emission of a lower energy photon due to incomplete absorption of the photon energy in addition to an electron ejection (Figure 33b).

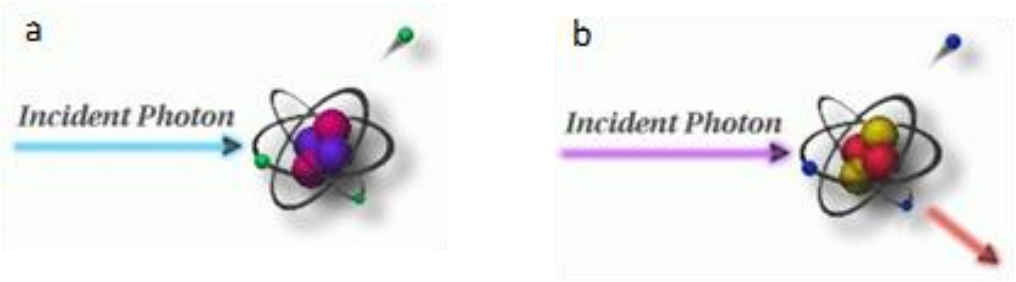

Figure 33: Photon interactions at varying energies. A) Photoelectric absorption, B) Compton scattering. Modified from Iowa State University Center for Nondestructive Evaluation (2021).

Medical grade CT scanners are typically calibrated to known standards, with the output being translated in CTN or Hounsfield Units (HU). Convention for HU defines air as -1,000 and water as 0. A linear transform of recorded HU values is performed to convert them into CTN. This study used CTN as it is the native export format for the instrument, but it is possible to use HU. Dual energy CT requires at least three calibration points and it is prudent to utilize standards that approximate the object or material of interest. Pure samples of aluminum, graphite, and sodium chloride were used as the calibration standards as they most closely approximate the rocks and minerals of interest (Table 3). Most materials denser than water or with higher atomic masses have a non-linear response to differing CT energies (Table 4).

Table 3: Dual Energy Calibration Standards, Bulk Density (gm/cm^3)

Material	ρ_B (g/cm^3)
Air	-0.001
Water	1
Graphite	2.3
Sodium Chloride	2.16
Aluminum	2.7

Table 4: Dual Energy Calibration Standards, HU and CTN for "Low" and "High" Energies

Material	HU		CTN	
	80 KeV	135 KeV	80 KeV	135 KeV
Air	-993	-994	31,775	31,774
Water	-3.56	-2.09	32,764	32,766
Graphite	381	437	33,149	33,205
Sodium Chloride	1,846	1,237	34,614	34,005
Aluminum	2,683	2,025	35,451	34,793

Dual energy CT utilizes these differences to calibrate to the X-ray spectra. Two equations with three unknowns each are utilized to find ρ_B (Siddiqui and Khamees, 2004):

$$\rho_B = mCTN_{low} + pCTN_{high} + q$$

$$Z_{eff} = \sqrt[3.6]{\frac{(rCTN_{low} + sCTN_{high} + t)}{(0.9342 * \rho_B + 0.1759)}}$$

Where [m, p, and q] and [r, s, and t] are unknown coefficients that can be solved by setting up a system of equations with four 3 x 3 determinants. The CTN is obtained from the CT scans for each of the homogenous calibration standards.

In this study the high and low energy image stacks were loaded into Python as arrays. A 3D Gaussian blur filter with a sigma of 2 was used to reduce noise in the images. The scipy.solv module of Python was then employed to solve for the coefficients based on the calibration of CTN values. The ρ_B was solved for each pixel in the 3D volume and saved as two new separate image stacks. The Z_{eff} was solved for at each pixel as well, and the data is available on the EDX data page.

3.5 COMPILED CORE LOG

The compiled core logs were scaled to fit on single pages for rapid review of the combined data from the medical CT scans and MSCL readings. Two sets of logs are presented; the first set with data from the major elements and elemental ratios, and the second set with elemental proxies and CT image data (Zeff and Dual Energy Density). Features that can be derived from these combined analyses include determination of mineral locations, such as pyrite, from magnetic susceptibility. The XRF is used to inform on geochemical composition and mineral form.

Data from the MSCL was filtered to remove areas of fractures and missing core, P-wave velocity was limited to values greater than 330 m/s, gamma density (and dual energy density) were limited to values greater than 1.5 g/cm^3, and Zeff was limited to values greater than 12.

The elemental results from the XRF were limited to major elements (LE, Ca, Si, Al) and elemental proxies related to redox potential (Co, Ni, Cu, and V), biogenic production (P and V*),

skeletal influx/carbonate potential (Ca and Mn), detrital influence (Zr, Ti, Al, Si), and chalcophiles (Pb, S, Fe).

Trends in elemental ratios can provide insight into mineral composition, oxidation state, and depositional setting. Examples include: Ca/Si, which provides information on relative abundance of calcium carbonates versus silicates; Mn/Fe, which provides information on oxidation, where a decrease in the ratio is related to zones of anoxic/euxinic conditions and an increase is related to zones of dysoxic/oxic conditions; S/Fe which provides information on the abundance of pyrite (and other iron sulfates) versus Fe oxide minerals; Fe/Al, which provides information about the degree of pyritization in shales; Ti/Al, which provides information about terrigenous input; and Si/Al, which provides information on the abundance of illite and micas versus other clays. Magnetic susceptibility can test for iron sulfides (reducing) or oxidized Fe and sulfate. The elemental proxy log also includes an XRF "mineralogy" with Al, representing clays; Ca, representing calcite; and Si, representing only quartz, although there is some Si contribution to the clays. Zeff is also displayed where ~14 represents carbonate-rich facies, ~13 represents clay rich facies, and ~12 represents quartz-rich facies. Pyrite (reduced) should have low magnetic susceptibility, and Fe oxide or hydroxide should have high magnetic susceptibility. These broad trends can quickly give information on large suites of core and direct more focused research. These logs are presented in the following images (Figure 34 to Figure 35).

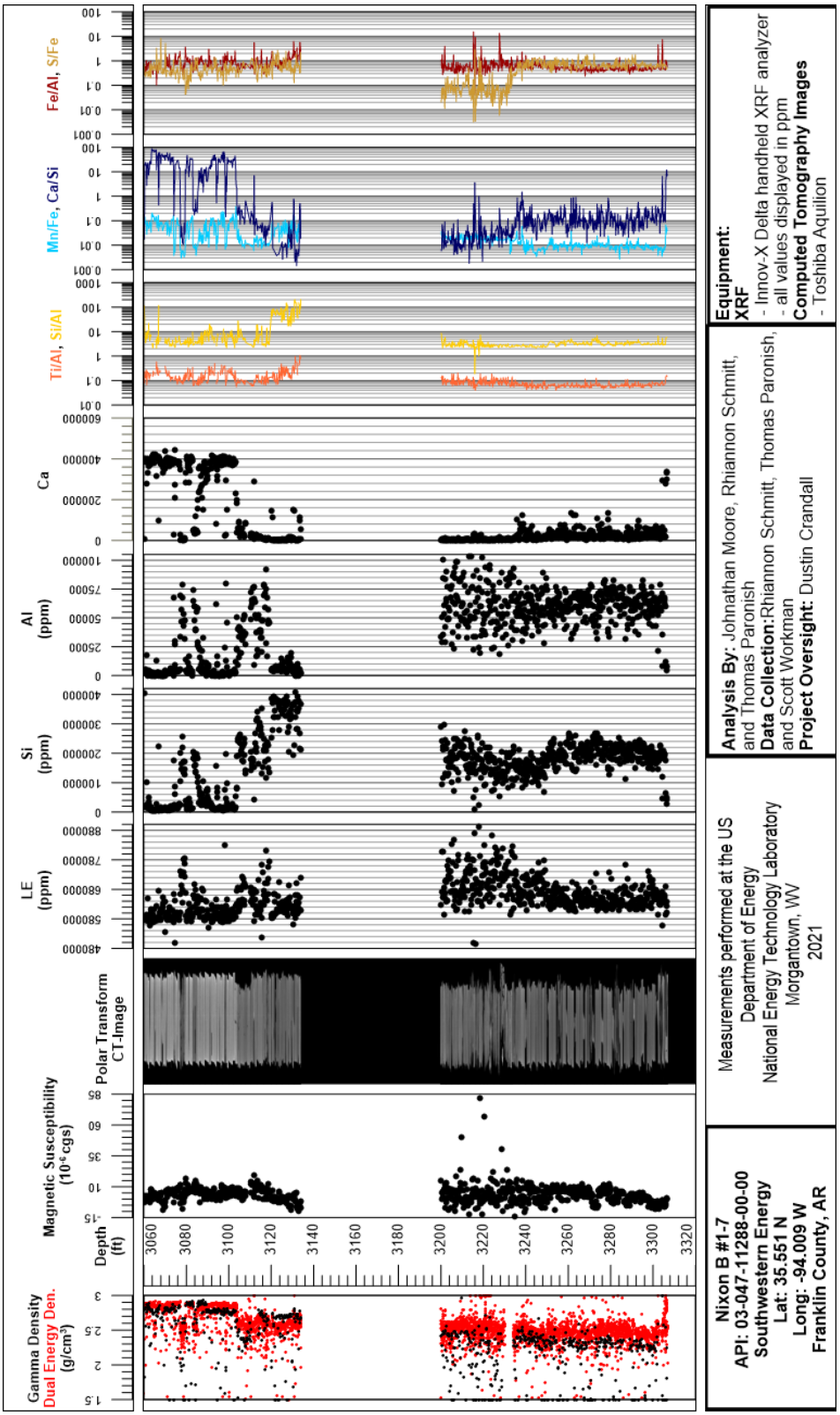

Figure 34: Compiled core log for Nixon B #1-7 with major elements and elemental ratios, from 3,060 to 3,310 ft.

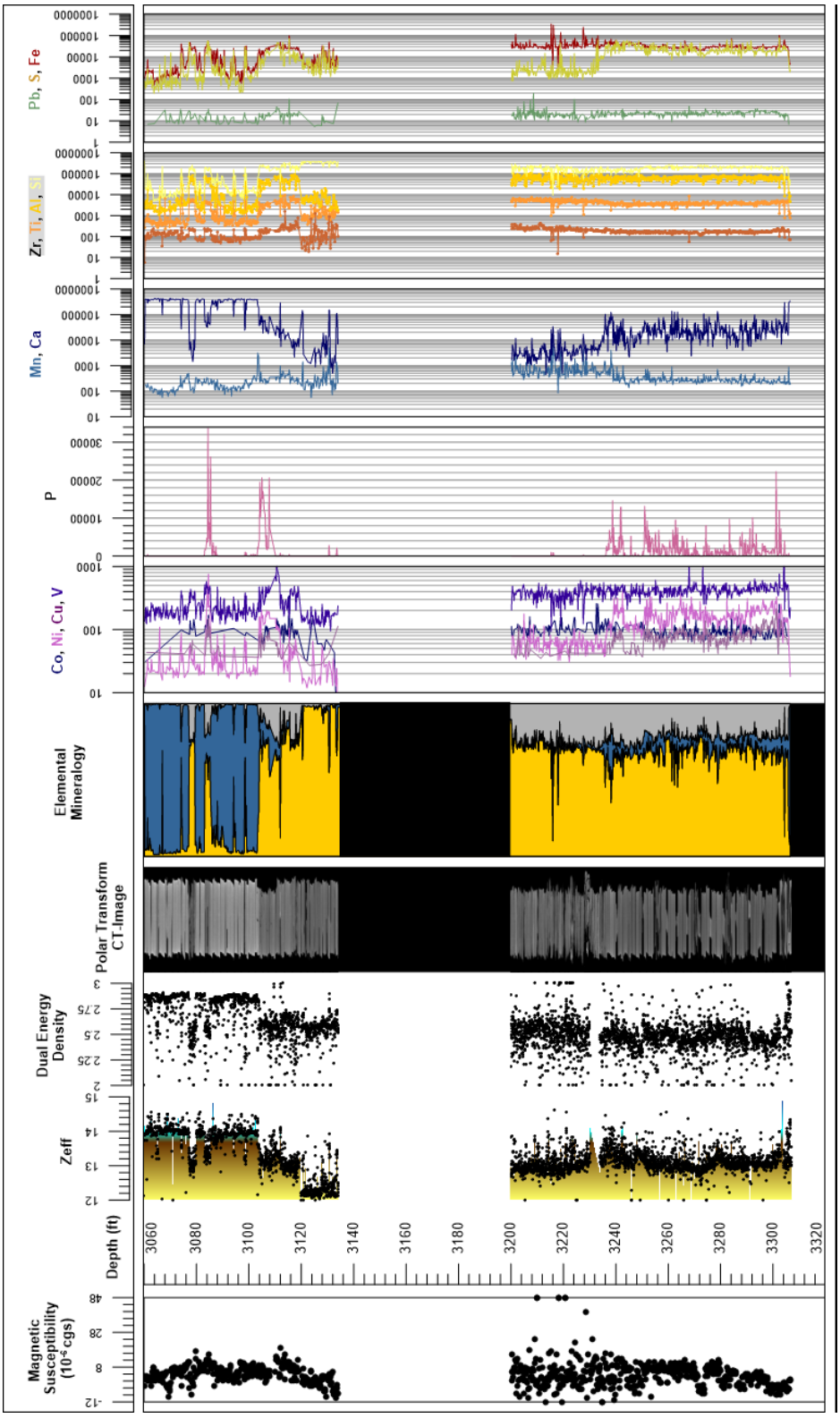

Figure 35: Compiled core log with elemental proxies for Nixon B #1-7, from 3,060 to 3,310 ft.

4. DISCUSSION

The measurements of the magnetic susceptibility, P-wave velocity, XRF, and CT analysis provide a unique look into of the internal structure of the core and macroscopic changes in lithology. These techniques:

- Are non-destructive
- When performed in parallel give insight into the core beyond what one individual technique can provide
- Can be used to identify zones of interest for detailed analysis, experimentation, and quantification
- Provide a detailed digital record of the core, before any destructive testing or further degradation, that is accessible and can be referenced for future studies.

5. REFERENCES

Crandall, D.; Moore, J.; Rodriguez, R.; Gill, M.; Soeder, D.; McIntyre, D.; Brown, S. *Characterization of Martinsburg Formation using Computed Tomography and Geophysical Logging Techniques*; NETL-TRS-4-2017; NETL Technical Report Series; U.S. Department of Energy, National Energy Technology Laboratory: Morgantown, WV, 2017; 68.

Geotek Ltd. Geotek Multi-Sensor Core Logger Flyer, Daventry, UK, 2009. http://www.geotek.co.uk/sites/default/files/MSCLOverview.pdf

Geotek Ltd. Multi-Sensor Core Logger Manual; Version 05-10; Published by Geotek, 3 Faraday Close, Daventry, Northamptonshire NN11 8RD, 2010. info@geotek.co.uk, www.geotek.co.uk

Houseknecht, D.W. Evolution from passive margin to foreland basin: the Atoka formation of the Arkoma basin, south-central USA. *Foreland basins* **1986,** 327–345.

Hunts, C.; Moskowitz, B.; Banerjee, S. *Magnetic Properties of Rocks and Minerals;* Rock Physics and Phase Relations: A Handbook of Physical Constants; 1995; 189–204.

Iowa State University Center for Nondestructive Evaluation, Ames, IA, 2021. https://www.nde-ed.org/Physics/X-Ray/attenuation.xhtml (accessed July 2021).

Johnson, T. R. C. Dual-Energy CT: General Principles. *American Journal of Roentgenology* **2012,** *199*(5_supplement), S3–S8. DOI: 10.2214/AJR.12.9116.

McGilvery, T. A.; Manger, W. L; Zachry, D. L. Summary and guidebook to the depositional and tectonic history of the Carboniferous succession Northwest Arkansas. In *AAPG Midcontinent Section Meeting field trip;* 2016.

Schneider, C. A.; Rasband, W. S.; Eliceiri, K. W. NIH Image to ImageJ: 25 years of image analysis. *Nature Methods* **2012,** *9*, 671–675.

Siddiqui, S.; Khamees, A. A. Dual-Energy CT-Scanning Applications in Rock Characterization. *Society of Petroleum Engineers* **2004**. DOI:10.2118/90520-MS.This page intentionally left blank.

Brian J. Anderson
Director
National Energy Technology Laboratory
U.S. Department of Energy

Jared Ciferno
Associate Director
Oil and Gas
Technology Development & Integration Center
National Energy Technology Laboratory
U.S. Department of Energy

Elena Melchert
Director
Division of Upstream Oil and Gas Research
U.S. Department of Energy

Bryan Morreale
Executive Director
Research and Innovation Center
National Energy Technology Laboratory
U.S. Department of Energy

NETL Technical Report Series